의학박사 학위논문

Multiplex Molecular Target Detection in a Colorectal Cancer Xenograft Model Utilizing Simultaneous Fluorescence-Raman Endoscopic System

대장직장암 마우스 모델에서

형광-라만 동시 내시경 영상을 이용한

실시간 다중복합 생체분자진단

2016 년 2 월

서울대학교 융합과학기술대학원

분자의학 및 바이오제약학과

김 용 일

Multiplex Molecular Target Detection in a Colorectal Cancer Xenograft Model Utilizing Simultaneous Fluorescence-Raman Endoscopic System

지도교수 이 동 수

이 논문을 의학박사 학위논문으로 제출함
2015 년 11 월

서울대학교 융합과학기술대학원
분자의학 및 바이오제약학과
김 용 일

김용일의 의학박사 학위논문을 인준함
2015 년 12 월

위 원 장 김 성훈 (인)
부위원장 이 동수 (인)
위 원 정 대홍 (인)
위 원 이 윤상 (인)
위 원 오 도연 (인)

Abstract

Multiplex Molecular Target Detection in a Colorectal Cancer Xenograft Model Utilizing Simultaneous Fluorescence-Raman Endoscopic System

Yong-il Kim

Department of Molecular Medicine and Biopharmaceutical Science,

The Graduate School of Convergence Science and Technology,

Seoul National University

Purpose:

Fluorescence endomicroscopy provides quick access to molecular targets, while Raman spectroscopy allows the opportunity to detect multiplex molecular targets. We have developed a simultaneous fluorescence-Raman endoscopic system (FRES) and herein demonstrate its value in an orthotopic colorectal cancer (CRC) xenograft model. In this study, we identified multiplex targeting ability (both tumor cell and tumor microenvironment targeting), applicability in a real-time endoscopic

model, sensitivity, and quantification possibility of the FRES.

Methods:

The FRES was constructed by modifying a commercialized confocal laser endomicroscope to provide simultaneous fluorescence and Raman signals in real-time. In a CRC xenograft model, epidermal growth factor receptor (EGFR) and vascular endothelial growth factor (VEGF) were targeted with antibody-conjugated fluorescence and surface-enhanced Raman scattering nanoprobes (F-SERS dots) to evaluate the efficacy of the FRES. In addition, we assessed the multiplex molecular targeting ability in a real-time endoscopic model. Moreover, we established subcentimeter-sized small CRC model and identified sensitivity by reducing the F-SERS dots.

Results:

Simultaneous fluorescence and Raman signals detection was achieved by the FRES. The FRES was useful for fast signal detection [by fluorescence signal; Alexa Fluor (AF) 610] and multiplex targeting [by Raman signals; rhodamine B isothiocyanate (RITC) and fluorescein isothiocyanate (FITC)] using EGFR and VEGF antibody-conjugated F-SERS dots in an orthotopic CRC xenograft model on tumor-exposed and real-time endoscopic systems. In addition, the FRES showed a multiplex targeting ability, even in a subcentimeter-sized CRC, using a half spraying dose of antibody-conjugated F-SERS dots. Raman signal intensity was quantified by measuring highest height of Raman signal, and showed linear

increased tendency according to dose of antibody-conjugated F-SERS dots, seeded cell density and expression of molecular characteristics.

Conclusions:

Our results demonstrate that FRES showed fast signal detection and a multiplex targeting ability by fluorescence and Raman signals, respectively. By the FRES, tumor cell (EGFR in CRC cell membrane) and tumor microenvironment (VEGF in extracellular matrix) could be simultaneously assessed, and can be applied to real-time endoscopic system. In addition, the multiplex targeting ability of FRES was applicable even to subcentimeter-sized tumors at a low concentration of F-SERS dots (5 nmole). The toxicity of the nanoprobes used can be reduced by using a nontoxic coating, as well as a topical spray, and by a dose reduction in antibody-conjugated F-SERS dots. Lastly, Raman intensity could be quantified and showed the possibility to measure the molecular heterogeneity of the tumor.

Keywords: fluorescence; Raman; multiplex targeting; endoscopy; colon cancer; surface-enhanced Raman scattering

Student Number: 2009-24111

Contents

List of Figures

List of Tables

List of Abbreviations

Full name	Abbreviations
fluorescence-Raman endoscopic system	FRES
colorectal cancer	CRC
epidermal growth factor receptor	EGFR
vascular endothelial growth factor	VEGF
fluorescence and surface-enhanced Raman scattering nanoprobes	F-SERS dots
Alexa Fluor	AF
confocal laser scanning microscopy	CLSM
surface-enhanced Raman scattering nanoparticles	SERS dots
positron emission tomography	PET
computed tomography	CT
magnetic resonance imaging	MRI
tetraethylorthosilicate	TEOS

3-mercaptopropyltrimethoxysilane	MPTS
ethylene glycol	EG
aminopropyltriethoxysilane	APTES
octylamine	OA
rhodamine B isothiocyanate	RITC
fluorescein isothiocyanate	FITC
dimethyl sulfoxide	DMSO
N-methyl-2-pyrrolidone	NMP
N-hydroxysuccinimide	NHS
N,N′-diisopropylcarbodiimide	DIC
N,N′-diisopropylethylamine	DIPEA
4-dimethylaminopyridine	DMAP
bovine serum albumin	BSA
phosphate-buffered saline	PBS
deionized	DI
nanoparticles	NPs

nanoparticle tracking analysis	NTA
internal ribosomal entry site	IRES
radio-immunoprecipitation assay	RIPA
regions of interest	ROIs
tumor-to-background ratio	TBR
counts per second	CPS
4', 6-diamino-2-phenylindole	DAPI
immunohistochemistry	IHC
avidin–biotin complex	ABC
hematoxylin and eosin	H&E
transmission electron microscopy	TEM
standard deviation	SD
arbitrary unit	a.u.
human epidermal growth factor receptor-2	HER2

Introduction

Colonoscopy (standard white light endoscopy) is an essential tool for the localization of colorectal cancer (CRC) and the excision of suspected neoplastic lesions by surgery (*1,2*). However, colonoscopy for CRC may result in a misdiagnosis in up to 25% of cases, and polyps without malignant potential could be treated with high risk and cost to the patient (*3*). Technological advancements in endoscopy procedures have improved endoscopic diagnosis with a high accuracy of cancer detection and with a reduction in frequency of inappropriate endoscopic treatment. Some examples of such endoscopy improvements include chromoendoscopy, light-scattering spectroscopy, autofluorescence imaging, endocystoscopy, and high-resolution and magnifying endoscopy, etc (*4*).

Recently, molecular imaging has emerged as a new endoscopic method, which provides an opportunity for the early detection of molecular targets and allows personalized therapy. Fluorescence-based endomicroscopy has recently been recognized as a potential cancer diagnostic approach in preclinical studies by providing microscopic images at the subcellular level using a fluorescent dye, and its territory has extended toward clinical practice as a tool of image-guided cancer surgery (*5*). Nevertheless, fluorescence-based endomicroscopy is restricted to one fluorescent dye at a time, which limits it in identifying the multiple characteristics of a cancerous lesion (*6*).

Another innovative technique is Raman spectroscopy, which is a good

candidate for gathering information about a lesion at the molecular level. Since each tissue contains biomolecules that have distinct vibrational energies in their molecular bonds, Raman spectroscopy can detect molecular components of the tissue, and hence subtle changes at a molecular level can be verified (*7,8*). Additionally, Raman spectroscopy with surface-enhanced Raman scattering nanoparticles (SERS dots) is capable of multiplex molecular imaging with high sensitivity (*9,10*), but its clinical value has not yet been fully tested (*4,11*).

Since each imaging modality has its own unique strengths and weaknesses, combinations of various imaging modalities have yet to be diligently explored. One of the most successful techniques is a combination of positron emission tomography (PET) and computed tomography (CT), mainly used in clinical oncology (*12*); also recently introduced is a combination of PET and magnetic resonance imaging (MRI) (*13*). Anatomical imaging (CT or MRI) is useful in the localization of lesions, and functional imaging (PET) provides molecular information about the local anatomy. In a similar vein, we would expect the combined use of fluorescence endomicroscopy and Raman spectroscopy to have an additive value from each modality – fluorescence endomicroscopy with its fast scanning of a lesion using a large field of view (*14*), and Raman spectroscopy with its multiplex molecular targeting ability (*15*) (Fig. 1).

For cancer progression, tumor cell need assistance from surrounding tumor microenvironment (fibroblasts, immune cells, blood vessels and extracellular matrix, etc.) Tumor microenvironment has been known to decide the extent of

tumor cell proliferation, angiogenesis, invasion and survival, so many molecular elements of the tumor microenvironment are emerging as attractive targets (*16*). And multi-targeted approach targeting tumor cell and tumor microenvironment may offer a more efficient way to treat cancer (*17*). Therefore, methods of imaging both tumor cell and tumor microenviroment is needed currently.

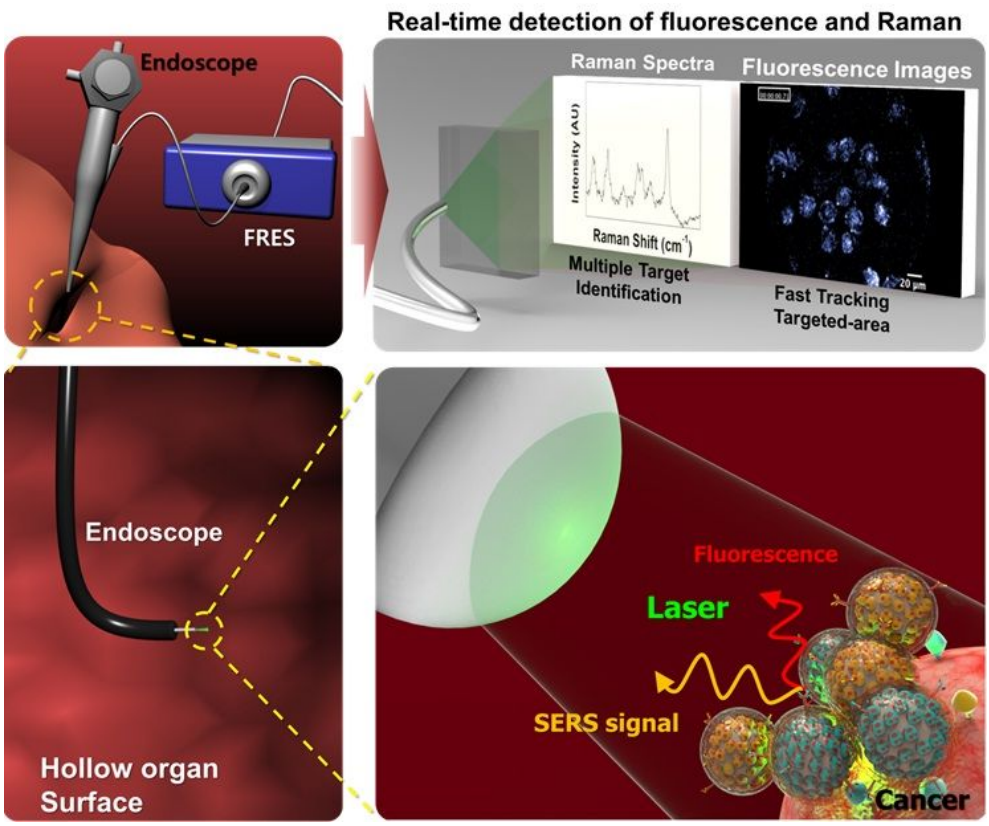

Figure 1. Illustration of a simultaneous fluorescence-Raman endoscopic system (FRES).

A fluorescence signal is used for fast detection of the tumor, and a Raman signal is used for multiplex targeting of the tumor.

Purpose

The aim of our study was to evaluate the usefulness of our simultaneous fluorescence-Raman endoscopic system (FRES) in a CRC xenograft model using fluorescence and surface-enhanced Raman scattering nanoprobes (F-SERS dots). Mutiplex targeting ability (both tumor cell and tumor microenvironment targeting), real-time endoscopic system applicability, sensitivity and quantification of Raman intensity studies were performed to validate the FRES.

Materials and Methods

Fluorescence-Raman endoscopic system (FRES)

The optical setup for FRES is fully described in a previous study (*18*). In brief, in order to simultaneously detect both fluorescence and Raman signals, FRES consisted of three units: 1) a dual-axis laser-scanning unit, 2) a separation unit, and 3) a signal-detecting unit (Fig. 2). The dual-axis laser-scanning unit (Raman prototype of Cell-Vizio^{TM}; Mauna Kea Technologies, Paris, France) had two orthogonally oscillating mirrors that were allowed to sequentially inject a laser into each optical fiber bundle for light incidence. To introduce the laser to the sample and collect signals from the sample, optical fiber bundles having a 2.6 mm external diameter, a 60 μm working distance, and a 240 μm field of view were utilized. As an excitation source, a continuous wave diode-pumped solid-state 532 nm laser (Cobolt Samba^{TM}; Cobolt AB, Solna, Sweden) was used, coupled with a single mode fiber. The separation unit used two optical filters: a long-pass dichroic filter (FF593-Di03-25D; Semrock Inc., Rochester, NY, USA) for separating the fluorescence signal from the collected signal, and an edge filter (LP03-532RS-25; Semrock Inc., Rochester, NY, USA) for the separation of Rayleigh- and Raman-scattering of light. To simultaneously provide real-time fluorescence images and Raman spectra, the signal detecting unit consisted of two independent detectors: a spectrometer (SR 303i-A; Andor Technology, Belfast, UK) with a thermo-electrically cooled CCD detector (DV401A-BV; Andor Technology, Belfast, UK)

for Raman signal detection and an avalanche photodiode for fluorescence signal detection. The collected fluorescence signals were processed into real-time fluorescence images by imaging software (ImageCell; Mauna Kea Technologies, Paris, France).

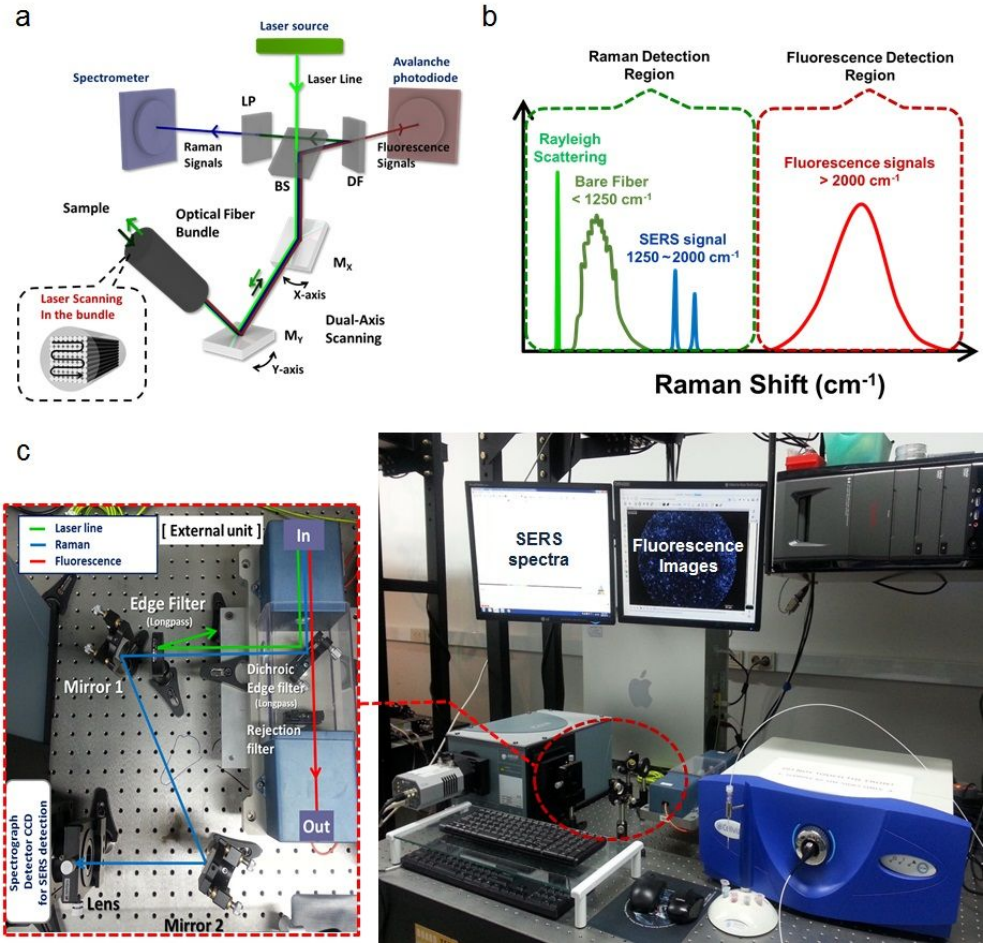
a
Laser source
Spectrometer
Laser Line
Avalanche photodiode
LP
Raman Signals
Fluorescence Signals
BS
DF
Sample
Optical Fiber Bundle
M_X
X-axis
Laser Scanning In the bundle
Dual-Axis Scanning
M_Y
Y-axis
b
Raman Detection Region
Fluorescence Detection Region
Rayleigh Scattering
Bare Fiber < 1250 cm-1
SERS signal 1250 ~ 2000 cm-1
Fluorescence signals > 2000 cm-1
Raman Shift (cm-1)
c
Laser line
Raman
Fluorescence
[External unit]
In
Edge Filter
(Longpass)
Mirror 1
Dichroic Edge filter
(Longpass)
Rejection filter
Out
Spectrograph Detector CCD for SERS detection
Lens
Mirror 2
SERS spectra
Fluorescence Images

Figure 2. Description of devices and optical results for the FRES.

(a) A schematic diagram of the optical beam path (Mx: oscillating mirror for the X-axis, My: oscillating mirror for the Y-axis, BS: beam splitter, DF: dichroic filter, and LP: long pass Raman edge filter) (b) An illustration of the spectrum of collected lights from the FRES. The collected lights contained four different kinds of signals: 1) scattered laser-line (Rayleigh scattering) 2) a Raman scattering signal due to intrinsic bare fiber, 3) fluorescence and 4) SERS signals from F-SERS dots. (c) Photograph of the FRES.

Chemicals and materials

Tetraethylorthosilicate (TEOS), 3-mercaptopropyltrimethoxysilane (MPTS), ethylene glycol (EG), silver nitrate ($AgNO_3$, > 99.99%), 3-aminopropyltriethoxysilane (APTES), octylamine (OA), rhodamine B isothiocyanate (RITC), fluorescein isothiocyanate (FITC), dimethyl sulfoxide (DMSO), *N*-methyl-2-pyrrolidone (NMP), *N*-hydroxysuccinimide (NHS), *N,N′*-diisopropylcarbodiimide (DIC), *N,N′*-diisopropylethylamine (DIPEA), 4-dimethylaminopyridine (DMAP), and bovine serum albumin (BSA, > 98%) were purchased from Sigma-Aldrich Inc. (St. Louis, MO, USA) and used without further purification. Ethanol (99.9% & 98 %), ammonium hydroxide (NH_4OH, 27%), and 2-propanol (99%) were purchased from Daejung Chemicals (Siheung, Korea). Succinimidyl esters conjugated with Alexa Fluor (AF) 610-X was purchased from Invitrogen Inc. (Carlsbad, CA, USA). Phosphate-buffered saline (PBS; 137 mM NaCl, 10 mM Na_2HPO_4, 2.0 mM KH_2PO_4, and 2.7 mM KCl at pH 7.4) was prepared in-house. Deionized (DI) water was used for all experiments. Cetuximab [anti-epidermal growth factor receptor (EGFR) monoclonal antibody] and Bevacizumab [anti-vascular endothelial growth factor (VEGF) monoclonal antibody] were purchased from Merck Millipore (Darmstadt, Germany).

Preparation of fluorescence surface-enhanced Raman scattering probes (F-SERS dots)

F-SERS dots were synthesized according to a previously reported method (*18*). Briefly, 200 nm-sized silica nanoparticles (NPs) were synthesized according to the Stöber method (*19*). TEOS (1.6 mL) in 40 mL of absolute ethanol was reacted with 3 mL NH_4OH for 20 h at room temperature. After thiol-functionalization on the surface of silica NPs (10 mg) by reacting 100 μL MPTS and 20 μL NH_4OH (27%) for 2 h at room temperature, silver NPs were directly introduced onto the surface of silica NPs by reducing 3 mM $AgNO_3$ in ethylene glycol with 10 mM octylamine for 1 h. To encode Raman label compounds, silver-embedded silica (Ag-Si) NPs were treated with 1 mM RITC or 1 mM FITC, respectively. The Raman-labeled Ag-Si NPs were then encapsulated in a silica shell using TEOS and NH_4OH. Further encapsulation in a fluorescence dye (AF 610)-conjugated silica shell was performed in a TEOS (10 μL), NH_4OH (0.5 mL, 27%), and AF610-APTES (55 μL) conjugated solution, which was previosuly prepared by reacting 5 μL AF610 (8 mM in DMSO) with 50 μL APTES (19.2 mM in ethanol) for 15 h. The final synthesized nanoprobes [F-SERS dots-A (by RITC) and -B (by FITC)] were washed with ethanol several times for purification purposes, and then redispersed in ethanol.

Immobilization of antibodies on F-SERS dots

To introduce an amino-functional group on the surface of F-SERS dots, 1 mg of F-SERS dots was treated with a 1 mL APTES solution (5% volme in ethanol) and 10 μL NH_4OH (27%) for 1 h at room temperature. After washing with ethanol, the amine-functionalized F-SERS dots (1 mg) were then reacted with 1.75 mg succinic anhydride and 3 μL DIPEA in 500 μL NMP for 2 h to introduce carboxylic acid groups. Subsequently, the carboxylic acid group-functionalized F-SERS dots were activated with 2 mg NHS, 2.7 μL DIC, and 0.21 mg DMAP for 2 h. To remove excess reagents, the resulting solution was centrifuged and washed with NMP and PBS (pH 7.4). For antibody conjugation, cetuximab (50 μg) or bevacizumab (50 μg) was added to the NHS-activated F-SERS dots-A/B dispersed in 200 μL of PBS, respectively. After incubation for 1 h at room temperature, antibody-immobilized F-SERS dots were centrifuged and washed with PBS containing 0.1% (w/v) Tween 20, and then with PBS, consecutively. Finally, to improve bio-compatibility, antibody-immobilized F-SERS dots were treated with BSA [1% (w/v) in PBS solution, pH 7.4] for 30 min, washed with PBS solution containing Tween 20, and then with PBS as above.

Size and concentration measurements

Size distribution was measured using the nanoparticle tracking analysis (NTA) method (NanoSight NS500; Malvern, Worcestershire, UK). Samples were diluted sufficiently for contrast and to minimize background. A quick measurement mode was performed to find optimal conditions. Then, a total of five particle

motion videos were recorded automatically using a standard measurement mode. Captured videos (five videos per sample) were processed and analyzed. All other conditions were constant. Graphical figures were automatically drawn by software.

Establishment of colorectal cancer cell lines and their evaluation

The human colorectal adenocarcinoma cell line (HT29), which is known to express EGFR and VEGF (*20*), was acquired from the Korean Cell Line Bank (KCLB, Seoul, Korea). HT29 cells were cultured in Dulbecco's Modified Eagle's Medium (DMEM; Invitrogen, Grand Island, NY, USA) supplemented with 10% fetal bovine serum, 100 U/mL penicillin and 100 g/mL streptomycin at 37°C in a humidified atmosphere containing 5% CO_2. A retroviral vector containing codon-optimized firefly luciferase complementary DNA (effluc), and Thy1.1 (CD90.1), which is linked with an internal ribosomal entry site (IRES), was constructed for enhanced bioluminescence cell imaging (*21,22*). HT29 cells were transfected with a recombinant retroviral vector encoding a luciferase gene (HT29-effluc). To determine whether the luciferase gene was expressed in established HT29-effluc cells, HT29-effluc cells were seeded into a 24-well plate, and an *in vitro* luciferase assay was performed according to the seeded cell number and protein concentration using a luminometer (TR717p; Applied Biosystems, Grand Island, NY, USA). Protein concentrations were measured using BCA protein assay kits (Thermo Scientific, Rockford, IL, USA).

Western blot analysis

Cells were lysed in radio-immunoprecipitation assay (RIPA) buffer (Sigma, St. Louis, MO, USA) containing protease inhibitor cocktail (Roche Diagnostics, Basel, Switzerland), and subsequently cleared via centrifugation (14,000 ×g for 20 min at 4°C). Protein concentrations were determined using BCA protein assay kits (Thermo Scientific, Rockford, IL, USA). Approximately 30 μg of protein was mixed with 4× polyacrylamide gel electrophoresis sample buffer, boiled at 70°C for 10 min, separated by gradient (4 – 12%) polyacrylamidegel electrophoresis, and transferred to nitrocellulose membranes (Invitrogen Grand Island, NY, USA). Membranes were blocked with 5% skim milk in Tris-buffered saline (20 mM Tris, 137 mM sodium chloride, and 0.1% polysorbate 20) for 1 h at room temperature, and then incubated overnight at 4°C with the following primary antibodies,: rabbit monoclonal EGFR antibody (1:1,000 dilution; Cell Signaling, Danvers, MA, USA), rabbit polyclonal VEGF antibody (1:1,000 dilution; Abcam, Cambridge, MA, USA) and mouse monoclonal β-actin antibody (1:5,000 dilution; Sigma-Aldrich, St. Louis, MO, USA). After membranes were washed three times with Tris-buffered saline, they were incubated with a secondary anti-rabbit/anti-mouse horseradish peroxidase–conjugated antibody (1:2,000 dilution; Santa Cruz Biotechnology, Santa Cruz, CA, USA) for 2 h, and enhanced chemiluminescence detection reagent (Thermo Scientific, Rockford, IL, USA). Signal intensities were then measured using an LAS-3000 imaging system (Fuji Film, Tokyo, Japan).

Modeling of orthotopic colorectal cancer (CRC) xenografts

All animal protocols were approved by the Institutional Animal Care and

Use Committee of the Seoul National University College of Medicine. Six-week-old male BALB/c nude mice were obtained from Orient Bio, Inc. (Seoul, Korea) and housed in a specific, pathogen-free environment. CRC xenograft mice were divided into three groups:

1) 1×10^7 of HT29-effluc cells injection, FRES imaging for a tumor-exposed system (n = 20; validation of the multiplex targeting ability of the FRES).

2) 1×10^7 of HT29-effluc cells injection, FRES imaging for an endoscopic system (n = 20; validation of the FRES in a real-time endoscopic system).

3) 5×10^6 of HT29-effluc cells injection, FRES imaging for a tumor-exposed system (n = 50; validation of the FRES sensitivity and the lower dose limit of antibody-conjugated F-SERS dots for a small tumor).

Before each tumor cell injection, mice were anesthetized with an intramuscular injection of 200 μL of 0.5% zoletil 50 (tiletamine-zolazepam; Virbac S.A., Carros, France) and 0.2% xylazine (Rompun; Bayer, Leverkusen, Germany) solution (1:1). Using a 30-gauge needle, a 0.1 mL volume of complex (containing tumor cells at a 1:1 ratio in medium/matrigel) was injected in to the posterior colorectal wall via the anus (*23,24*). Tumor growth was investigated for two weeks for the $1 \times 10^7$of HT29-effluc cells injection groups, and for one week for the 5×10^6 of HT29-effluc cells injection group.

Evaluation of orthotopic CRC xenograft model

Mice were followed up every two days after orthotopic CRC xenograft modeling and confirmed their survival. At the same time, mice were visually

examined for signs of anal erosion. For bioluminescence imaging acquisition, an IVIS100 imaging system (Caliper Life Sciences, Hopkinton, MA, USA) was used. D-luciferin potassium salt was diluted to 0.3 mg/mL in PBS before use, and 100 μL of the D-luciferin solution was intraperitoneally injected into mice. Mice were anesthetized with isoflurane and transferred into a light-tight chamber equipped with a charge-coupled device camera operated by Live Image software (Xenogen Corp., Alameda, CA, USA) to obtain bioluminescence images. Bioluminescence images were serially acquired every 5 min until maximum signals were reached (time: 1 s, binning: medium, f stop: 1). Signal intensities were displayed on a pseudocolor scale. To quantify emitted light, regions of interest (ROIs) were drawn on each bioluminescent image to quantify the optical flux (p/s/cm^2/sr, photons per second per cm^2 per steradian) over each tumor area. The same sized ROI was drawn for comparison over the brain area, and the tumor-to-background ratio (TBR; optical flux ratio between tumor and brain area) was calculated. Time points for bioluminescence image acquisition were one and two weeks for the 1×10^7 HT29-effluc cells injection groups, and one week for the 5×10^6 of HT29-effluc cells injection group.

In vitro and *in vivo* validation of the FRES

As a tumor targeting agent, antibody-conjugated F-SERS dots were measured in a conical tube, and fluorescence and Raman signals identified simultaneously. And the binding of antibody-conjugated F-SERS dots with colon

cancer cells was investigated. First, we identified the sensitivity and correlation of Raman intensity according to dose of antibody-conjugated F-SERS dots using FRES. HT29-effluc cells (10^4 cells/well) were seeded in an 8-well chambered cover glass (Lab-Tek; Thermo Scientific, Rochester, NY, USA) with 300 μL of cell media per well. After a 24 h incubation at 37°C, cells were fixed with 4% paraformaldehyde (Wako, Osaka, Japan) for 20 min, and washed three times with PBS. EGFR-F-SERS dots-A (0, 1, 5, 10, 20, 40, 80 and 100 μg) were added to a well, incubated at room temperature for 10 min, washed three times with PBS and FRES imaging was done for 3 min. In addition, we confirmed the FRES imaging difference according to seeded cell density (0, 10^3, 10^4, 10^5 cells/well) by 10 μg of EGFR-F-SERS dots-A in the same manner.

For *in vivo* studies, mice with CRC were initially anesthetized with an intramuscular injection of 200 μL of 0.5% zoletil 50 (tiletamine-zolazepam; Virbac S.A., Carros, France) and 0.2% xylazine (Rompun; Bayer, Leverkusen, Germany) solution (1:1). In a tumor-exposed system, after making an incision of the skin and anterior wall of the colorectal area, tumors were exposed and tumor sizes were measured using a digital caliper.

To validate the multiplex targeting ability of the FRES, 100 μg each of antibody-conjugated F-SERS dots (EGFR-F-SERS dots-A & VEGF-F-SERS dots-B, respectively) were sprayed onto the surface of a 1×10^7 HT29-effluc cell-injected tumor. After 10 min of incubation, antibody-conjugated F-SERS dots were washed five times with 300 μL of PBS. Simultaneous fluorescence and Raman

spectra of tumors were investigated in the tumor area by the FRES for 3 min. A single treatment with 100 μg each of antibody-conjugated F-SERS dots (EGFR-F-SERS dots-A or VEGF-F-SERS dots-B) or BSA-F-SERS dots-A/B (control) was also performed in the same manner.

To validate the FRES for a real-time endoscopic system, 100 μg of antibody-conjugated F-SERS dots were sprayed into the lumen of the colon through the anus. After 10 min of incubation, antibody-conjugated F-SERS dots treated areas were washed five times with 300 μL of PBS. The multiplexing capability of the FRES was investigated for 3 min by inserting a probe in the colon through the anus in tumor-implanted and normal mice.

To validate lower dose limit of antibody-conjugated F-SERS dots of the FRES in a small tumor, different amounts of antibody-conjugated F-SERS dots were sprayed onto the surface of a 5×10^6 HT29-effluc cell-injected tumor and evaluated by the FRES as above. The studied groups were as follows:

1) high dose: 100 μg each of EGFR-F-SERS dots-A and VEGF-F-SERS dots-B on the tumor,

2) medium dose: 50 μg each of EGFR-F-SERS dots-A and VEGF-F-SERS dots-B on the tumor,

3) low dose: 25 μg each of EGFR-F-SERS dots-A and VEGF-F-SERS dots-B on the tumor,

4) control: 100 μg each of EGFR-F-SERS dots-A and VEGF-F-SERS dots-B on the normal colon

The multiplex targeting ability of the FRES was graded into three levels: 1) “definite signal” occurred when two known Raman signals were definitely observed when a fluorescence signal was found [over 30 counts per second (cps) of both Raman signals],

2) “no signal” occurred when Raman and fluorescence signals were not observed (between 0 to 20 cps of either or both Raman signals),

3) “probable signal” occurred when the signals were between a definite and no signal state, which did not meet both criteria

These visual evaluations were performed in blinded conditions by the agreement of two examiners.

Confocal laser scanning microscopy (CLSM)

For *in vitro* analysis, the interaction of antibody-conjugated F-SERS dots with colon cancer cells was investigated. HT29-effluc cells (10^4 cells/well) were seeded in an 8-well chambered cover glass (Lab-Tek; Thermo Scientific, Rochester, NY, USA) with 300 μL of cell media per well. After a 24 h incubation at 37°C, cells were fixed with 4% paraformaldehyde (Wako, Osaka, Japan) for 20 min, and washed three times with PBS. Ten μg of antibody-conjugated F-SERS dots (EGFR-F-SERS dots-A, VEGF-F-SERS dots-B, and mixture) or BSA-F-SERS dots (control) were added to a well, incubated at room temperature for 10 min and then washed three times with PBS. Cell nuclei were stained by 4', 6-diamino-2-phenylindole (DAPI).

For *in vivo* analysis, tumors were excised, fixed with 4%

paraformaldehyde and sectioned, followed by the staining of nuclei using DAPI. Confocal laser scanning microscopy (CLSM: LSM 510 META; Carl Zeiss, Jena, Germany) was used for fluorescence signal detection. Excitation laser-lines for F-SERS dots and DAPI signals were 610 nm and 405 nm, respectively. Data were analyzed using LSM Image Examiner software (Carl Zeiss; Jena, Germany).

Pathologic evaluation

Immunohistochemistry (IHC) for EGFR and VEGF was carried out on formalin-fixed, paraffin-embedded serial sections cut at 3 μm and dried at 37°C overnight. Immunostaining was performed using an avidin–biotin complex (ABC) procedure, including heat-induced epitope and enzymatic antigen retrieval procedures. IHC for EGFR (C74B9 1:50; Cell Signaling Technologies, Beverly, MA, USA) and VEGF (VEGF-A20 1:100; Abcam, Cambridge, MA, USA) was performed according to manufacturer's instructions. Parallel sections were stained with hematoxylin and eosin (H&E).

Statistical analysis

The correlation between protein concentration and luciferase activity in the *in vitro* study was evaluated by Spearman's correlation. Statistical significance of *in vivo* bioluminescence studies was determined by a Wilcoxon signed rank test (TBR changes according to HT29-effluc cells injection week) a Mann-Whitney U test (TBR difference according to HT29-effluc cells injection number). A *P*-value less than 0.05 was considered significant. All statistical analyses were performed

using SPSS software (Version 18.0; SPSS Inc., Chicago, IL, USA) and MedCalc (Version 12.2; MedCalc Inc., Mariakerke, Belgium).

Results

Part I. Validation of F-SERS dots, FRES and colorectal cancer cells

Design of F-SERS dots and FRES

F-SERS dots-A and F-SERS dots-B which we synthesized was consisted of a silica core, Raman active chemicals for Raman signals, and a fluorescent silica shell for fluorescent signals as shown in Fig. 3. F-SERS dots-A and F-SERS dots-B were conjugated with corresponding antibodies (anti-EGFR or anti-VEGF, respectively), and exhibited a homogeneity in size, with mean diameters of 291.0 ± 87.4 nm and 296.6 ± 36.9 nm, respectively (Fig. 4 & Table 1). Antibody-conjugated F-SERS dots (EGFR-F-SERS dots-A and VEGF-F-SERS dots-B) were prepared in a conical tube, and fluorescence and Raman signals were measured by the FRES. Fluorescence signals observed in FRES were represented as small bright dots in FRES images, and Raman signals revealed a highest 1648 cm^{-1} Raman band for RITC (EGFR-F-SERS dots-A) and a 1324 cm^{-1} Raman band for FITC (VEGF-F-SERS dots-B) (Fig. 5). Antibody-conjugated F-SERS dots were postulated to be specifically attached to EGFR and VEGF positive HT29-effluc colon cancer cells in an orthotopic xenograft model. The FRES can detect fluorescence signals due to fluorescent silica shells (fast signal detection) and Raman signals due to Raman active chemicals on silver (multiplex targeting) (Fig. 6).

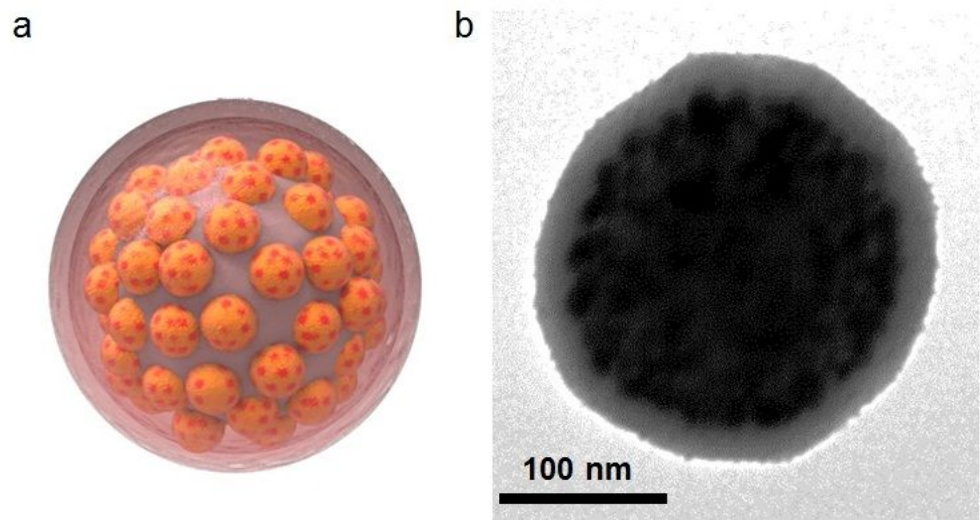

Figure 3. Characteristics of fluorescence and surface-enhanced Raman scattering nanoprobes (F-SERS dots).

Schematic (a) and transmission electron microscopy (TEM) images (b) showed a silica core, Raman active chemicals for Raman signals, and a fluorescent silica shell for fluorescent signals.

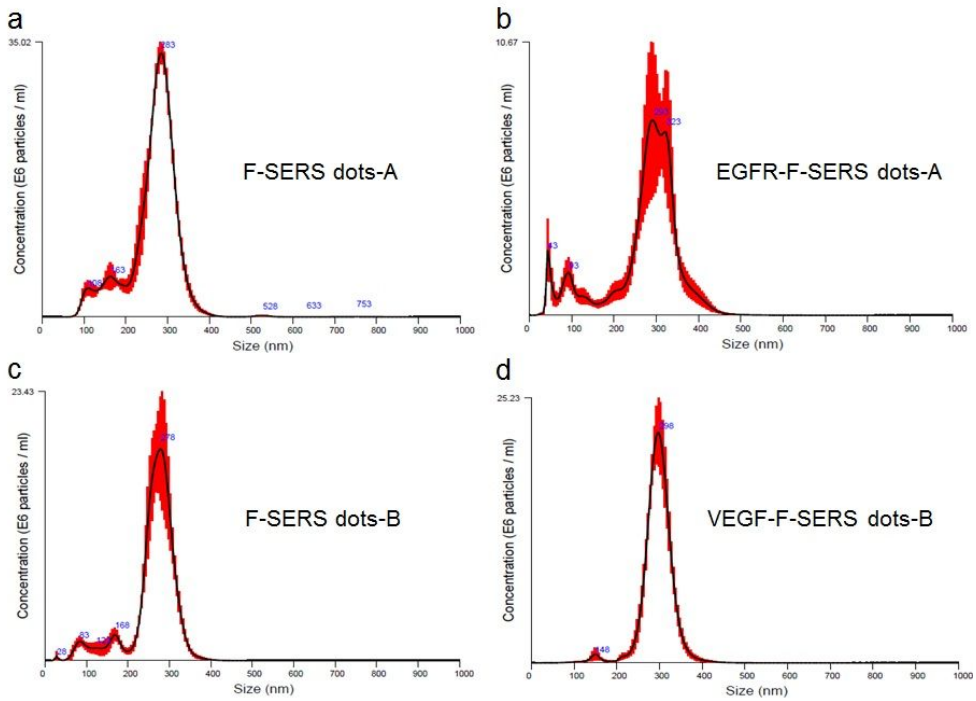

Figure 4. Size measurement of F-SERS dots and antibody-conjugated F-SERS dots.

The size of F-SERS dots-A were 284.4 ± 60.0 nm and EGFR-F-SERS dots-A were 291.0 ± 87.4 nm. And the size of F-SERS dots-B and VEGF-F-SERS dots-B were 278.1 ± 57.7 nm and 296.6 ± 36.9 nm, respectively.

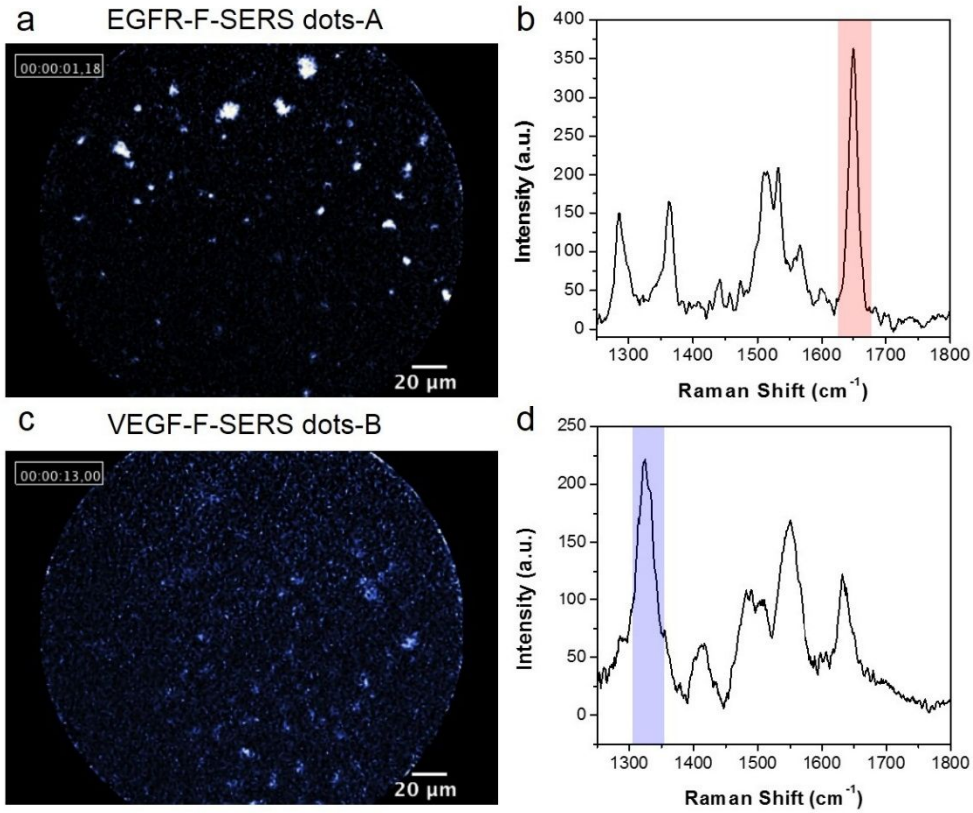

Figure 5. Evaluation of the FRES using antibody-conjugated F-SERS dots. Antibody-conjugated F-SERS dots (EGFR-F-SERS dots-A and VEGF-F-SERS dots-B) were prepared in a conical tube, and fluorescence and Raman signals were measured by the FRES. EGFR-F-SERS dots-A showed a small dotted fluorescence signal [Alexa Fluor (AF) 610, a] and a 1648 cm^{-1} intensity for the Raman signal (RITC, b).VEGF-F-SERS dots-B revealed small dotted fluorescence signals (AF 610, c) and 1324 cm^{-1} intensity for the Raman signal (FITC, d).

a.u. = arbitrary unit

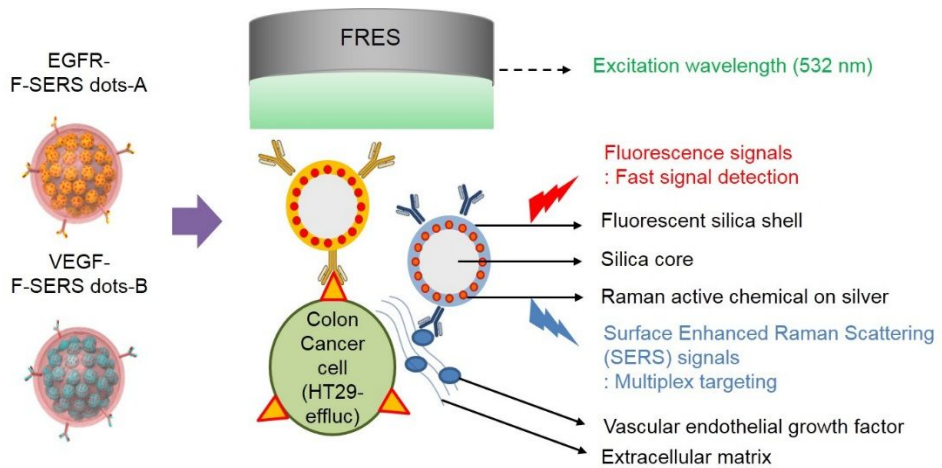

Figure 6. Schematic illustration of the FRES multiplex imaging using antibody-conjugated F-SERS dots.

When antibody-conjugated F-SERS dots were sprayed onto HT29-effluc colon cancer cells, antibody-conjugated F-SERS dots bound to colon cancer cell surface (EGFR) and tumor microenvironment (VEGF). The FRES uses the fluorescence signal of a fluorescent silica shell for fast signal detection (AF 610), and a Raman active chemical on silver allows Raman signals for multiplex targeting (RITC and FITC).

Characterization of colon cancer cell line and FRES in vitro

The HT29-effluc colon cancer cell line showed gradually increased luciferase activity with seeded cell number, and demonstrated a significant positive correlation with protein concentration ($R^2 = 0.987$, $P < 0.001$). Western blot analysis revealed EGFR and VEGF expression on HT29-effluc colon cancer cells (Fig. 7).

In vitro FRES study demonstrated that definite fluorescence and Raman signal was found from 5 μg ($10^4/cm^2$), saturation of Raman intensity was at 40 μg ($10^4/cm^2$), and FRES signal become definite as the seeded cell density increases (Fig. 8 & 9).

Antibody-conjugated F-SERS dots (EGFR-F-SERS dots-A and VEGF-F-SERS dots-B) were sprayed onto cultured colon cancer cells and their binding and uptake was evaluated using CLSM. When sprayed with 10 μg of antibody-conjugated F-SERS dots, the fluorescence signals of antibody-conjugated F-SERS dots were observed. However, when sprayed with 10 μg of BSA-F-SERS dots-A/B (control), the fluorescence signal was not seen (Fig. 10).

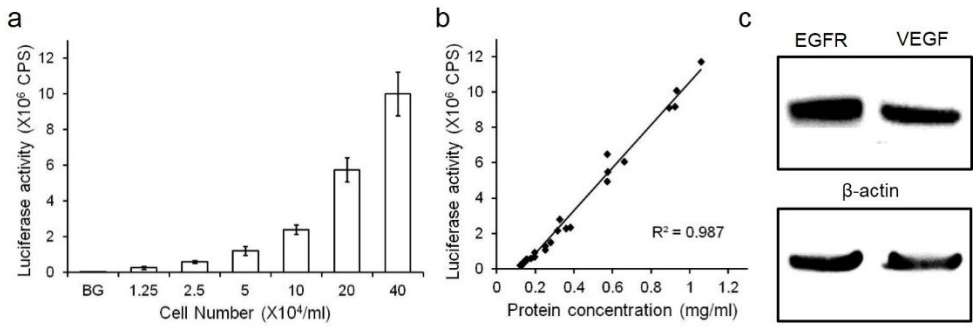

Figure 7. Characterization of HT29-effluc colon cancer cells.

HT29-effluc cells showed high luciferase activity according to seeded cell number (a) and a significant positive correlation with protein concentration ($R^2 = 0.987$, $P < 0.001$) (b). HT29-effluc cells demonstrated EGFR and VEGF expression by western blot analysis. The loading control used was β-actin (c).

CPS = count per sec.

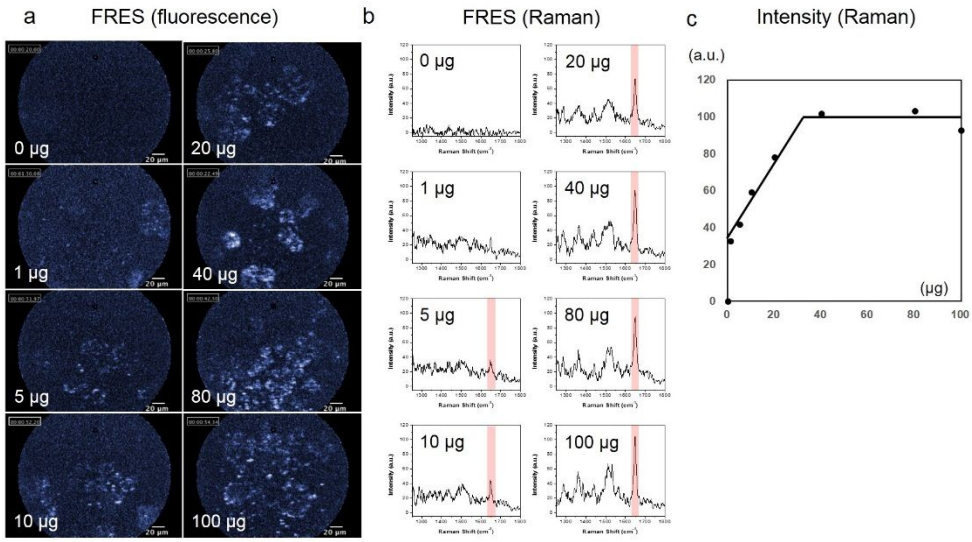

Figure 8. *In vitro* FRES result according to dose of EGFR-F-SERS dots-A.

By the FRES, definite EGFR-F-SERS dots-A binding to tumor cell could be found by fluorescence (a) and Raman (b) signals from 5 μg (10^4/cm^2). When Raman intensity at 1648 cm^{-1} were plotted (c), saturation was found at 40 μg (10^4/cm^2).

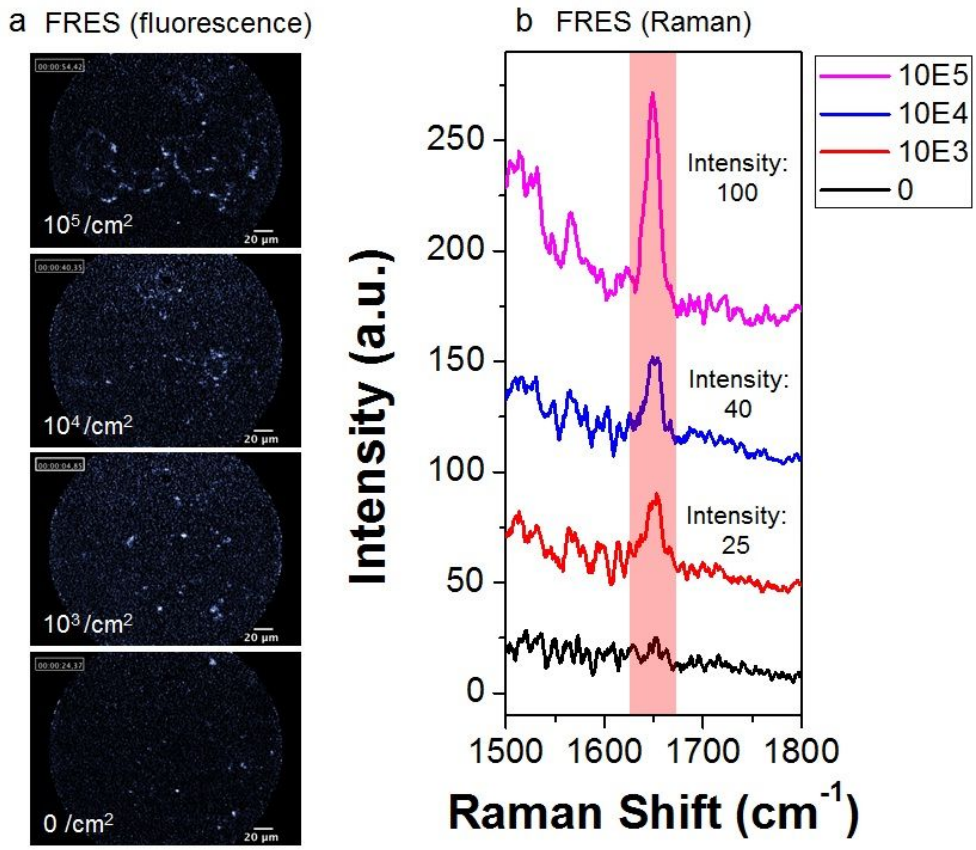

Figure 9. *In vitro* FRES according to seeded cell density.

Fluorescence signal (a) and Raman intensity at 1648 cm^{-1} (b) gradually become definite as the cell number increases.

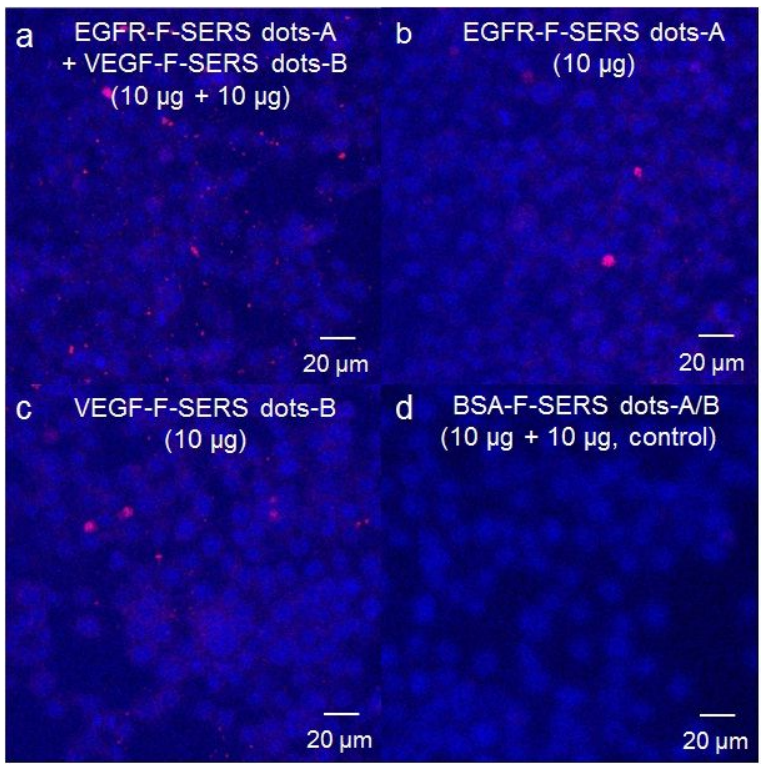

Figure 10. Confocal laser scanning microscopy (CLSM) after spraying 10 μg of antibody-conjugated F-SERS dots onto cultured HT29-effluc cells.
Dual (EGFR-F-SERS dots-A and VEGF-F-SERS dots-B) (a) or single (EGFR-F-SERS dots-A or VEGF-F-SERS dots-B, respectively) (b, c) spraying of antibody-conjugated F-SERS dots revealed the fluorescence signals, while BSA-F-SERS dots-A/B (control) showed no fluorescence signal (d). Cell nuclei were labeled with DAPI.

Part II. Multiplex targeting validation of the FRES

Orthotopic CRC xenograft modeling after 1 × 10^7 HT29-effluc cells injection

HT-29-effluc orthotopic CRC xenograft model was next established in BALB/c nude mice. Of 20 mice, 100% (20/20) of mice survived one week after a 1 × 10^7 HT29-effluc cells injection, and 70% (14/20) of mice survived after two weeks. Anal erosion symptoms (Fig. 11a) were found in 35% (7/20) of mice one week after injection and 86% (12/14) after two weeks (Table 2). All mice showed moderate-high luciferase activity after one week (100%, 20/20). The tumor-to-background ratio (TBR) two weeks after injection was significantly higher compared with the TBR one week after injection according to bioluminescence images (3354 ± 568 vs. 11021 ± 2400, $P = 0.002$*; Fig. 11b, c). The largest mean diameter of colon cancer tumors was 15 mm (range, 12 – 19 mm).

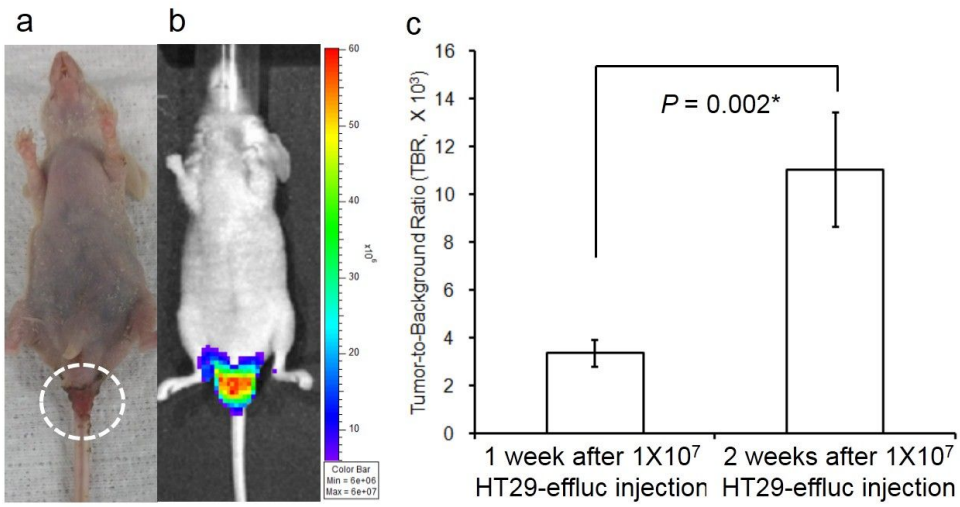

Figure 11. Orthotopic colorectal cancer (CRC) xenograft modeling for the FRES. Two weeks after 1×10^7 HT29-effluc cells injection in mice, anal erosion was found (a, white broken line) in most cases (86%, 12/14 mice). Bioluminescence imaging (b) showed moderate to high activity in the colorectal area. A significantly high tumor-to-background ratio (TBR, colorectal area/brain area) was identified at two weeks, compared with one week, after 1×10^7 HT29-effluc cells injection (11021 ± 2400 vs. 3354 ± 568, $P = 0.002$*; n = 14) (c).

Validation of multiplex targeting ability of the FRES

We next attempted to validate the targeting ability of the two synthesized antibody-conjugated F-SERS dots. A total of 14 mice with tumors induced by 1×10^7 HT29-effluc cells injection after 2 weeks prior were studied: five in multiplex targeting, six in single targeting (three for EGFR and three for VEGF) and three as controls (BSA-F-SERS dots). The FRES could simultaneously identify multiple bio-targets by fast fluorescence imaging and multiplex Raman spectral detection. The location of targeted F-SERS dots could be identified in real-time using AF610 fluorescence signals. At the same time, distinct SERS intensities for multiplex detection were observed at 1648 cm^{-1} and 1324 cm^{-1} in the Raman spectrum corresponding to RITC (EGFR-F-SERS dots-A) and FITC (VEGF-F-SERS dots-B), respectively (Fig. 12a, b). Definite signals were 80% (4/5) and probable signals were 20% (1/5) of mice for multiplex targeting abilities. A single spray of antibody-conjugated F-SERS dots demonstrated definite fluorescence and corresponding Raman (RITC or FITC) signals in all cases (Fig. 12c–f). In contrast, in all cases of spraying BSA-F-SERS dots-A/B as a control, none showed any fluorescence and Raman signals (Fig. 12g, h) (Table 3). As a counter confirmation experiment, CLSM experiments were performed on excised tumor, which showed definite binding of antibody-conjugated F-SERS dots to colon cancer cells, but a lack of binding of BSA-F-SERS dots (Fig. 13).

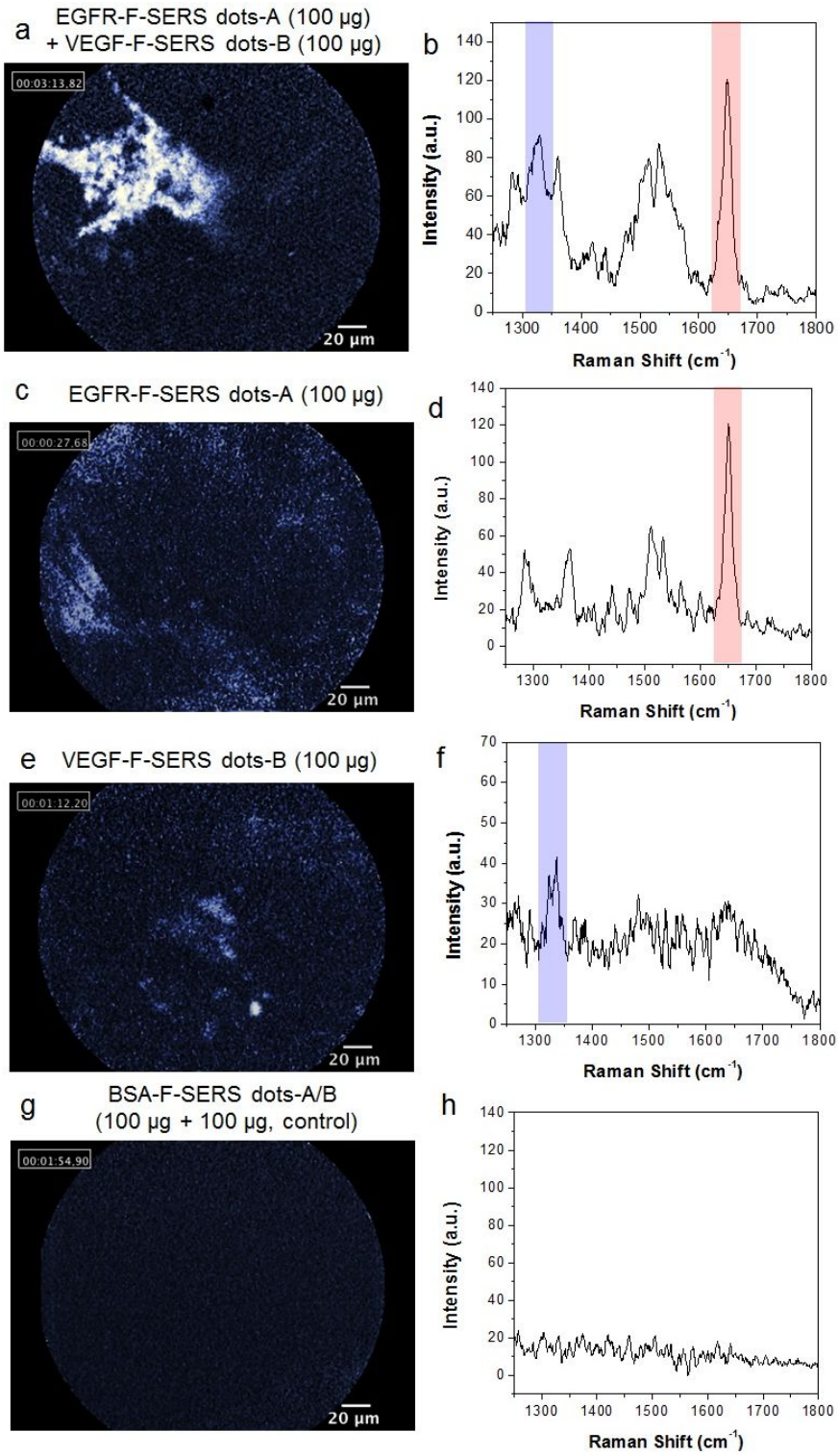
a
EGFR-F-SERS dots-A (100 μg)
+ VEGF-F-SERS dots-B (100 μg)
00:03:13.82
20 μm
b
Intensity (a.u.)
Raman Shift (cm-1)
c
EGFR-F-SERS dots-A (100 μg)
00:00:27.68
20 μm
d
Intensity (a.u.)
Raman Shift (cm-1)
e
VEGF-F-SERS dots-B (100 μg)
00:01:12.20
20 μm
f
Intensity (a.u.)
Raman Shift (cm-1)
g
BSA-F-SERS dots-A/B
(100 μg + 100 μg, control)
00:01:54.90
20 μm
h
Intensity (a.u.)
Raman Shift (cm-1)

Figure 12. FRES for multiplex targeting ability validation.

Mice were each subjected to 1×10^7 HT29-effluc cells injected tumor. After 2 weeks, an incision was made in the skin and anterior wall of the colorectal area, tumors were exposed and sprayed with antibody-conjugated F-SERS dots. After 10 min of incubation and PBS washing, tumors were investigated by a FRES probe. After spraying 100 μg of EGFR-F-SERS dots-A and 100 μg of VEGF-F-SERS dots-B, fluorescence signals were found by AF 610 (a), and two corresponding Raman signals were detected by RITC (A) and FITC (B) intensities (b). After a single spraying 100 μg of EGFR-F-SERS dots-A and 100 μg of VEGF-F-SERS dots-B, respectively, fluorescence signals (c, e) and corresponding single Raman signals [RITC (A) and FITC (B)] were found (d, f). In contrast, spraying of BSA-F-SERS dots-A/B demonstrated no definitive fluorescence (g) and Raman (h) signals.

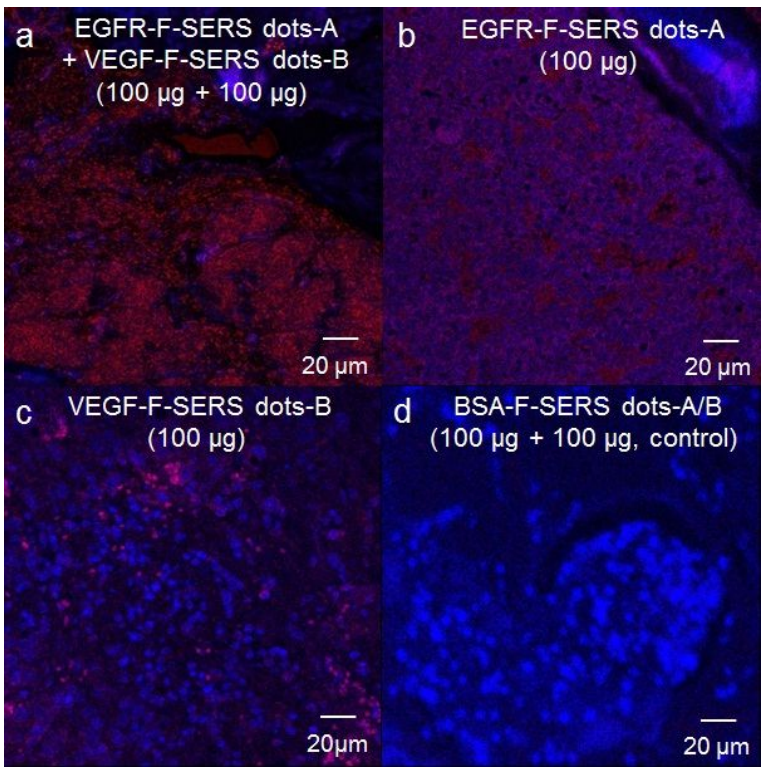

Figure 13. CLSM for the validation of multiplex targeting ability.

Tumors exposed to F-SERS dots in experiments for Fig. 12 were excised, fixed and sectioned. Nuclei were stained with DAPI. CLSM was used for fluorescence signal detection. Fluorescence signals were observed for both (a) and single (b, c) antibody-conjugated F-SERS dots sprayed on tumors. However, no signal was found for BSA-F-SERS dots-A/B sprayed on tumors (d).

Part III. Evaluation of FRES in a real-time endoscopic model

Orthotopic CRC xenograft modeling after 1 × 10^7 HT29-effluc cells injection in a real-time endoscopic system

We next used FRES imaging in a real-time endoscopic system of CRC xenograft model. Among 20 studied mice with colorectal cancer, all showed moderate-high luciferase activity one week after 1 × 10^7 HT29-effluc cells injection (100%, 20/20; Fig. 14a). The largest mean diameter of colon cancer was 13 mm (range of 11 – 17 mm), and FRES imaging in a real-time endoscopic system is shown (Fig. 14b).

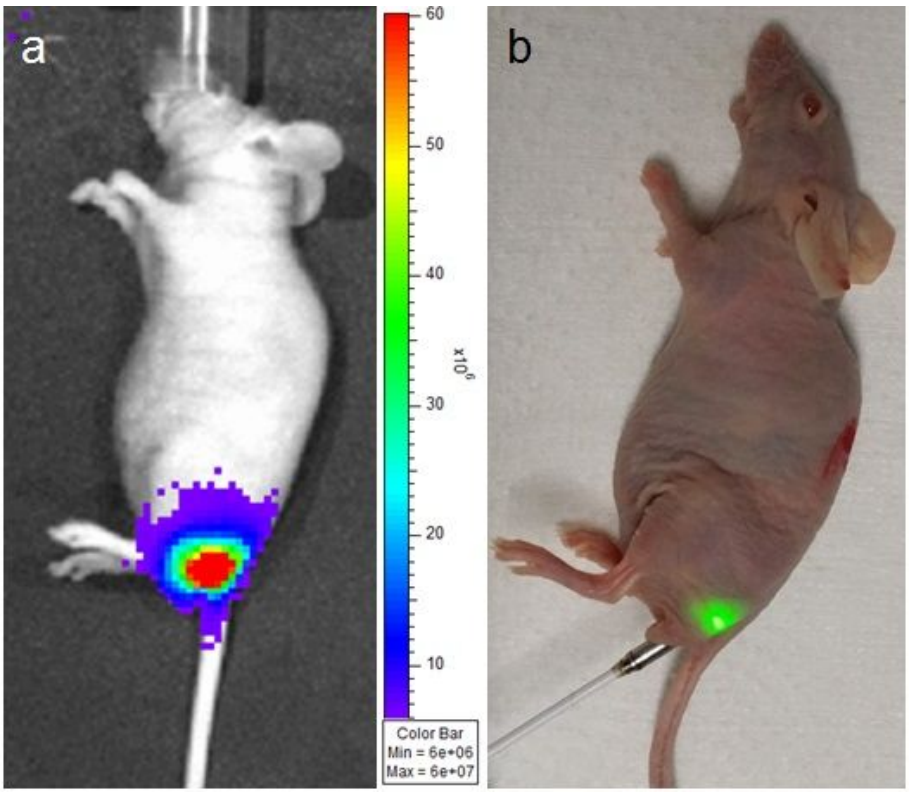

Figure 14. Orthotopic CRC xenograft modeling for a real-time endoscopic system. After one week of 1×10^7 HT29-effluc cells injection, bioluminescence imaging (a) showed moderate to high activity in the colorectal area of mice (lateral view; n = 20). The FRES imaging method on a real-time endoscopic system is shown (b).

Validation of the FRES in a real-time endoscopic system

We validated FRES imaging which utilized to detect tumors during real-time endoscopy. A total of 20 mice were investigated for a real-time endoscopic study of the FRES (EGFR-F-SERS dots-A 100 μg + VEGF-F-SERS dots-B 100 μg). In addition, 9 mice were studied as controls for normal colon (EGFR-F-SERS dots-A 100 μg + VEGF-F-SERS dots-B 100 μg). The FRES showed specific targeting ability with multiplexing capacity in all cases. Definite signals were observed in 75% (15/20), and probable signals in 25% (5/20), of mice with colorectal cancer (Fig. 15a, b). Fluorescence and Raman signals were not observed in the normal colon (Fig. 15c, d) (Table 4). H&E staining revealed tumor cell infiltration, and IHC results demonstrated both EGFR and VEGF positivity on exised colorectal cancer (Fig. 16).

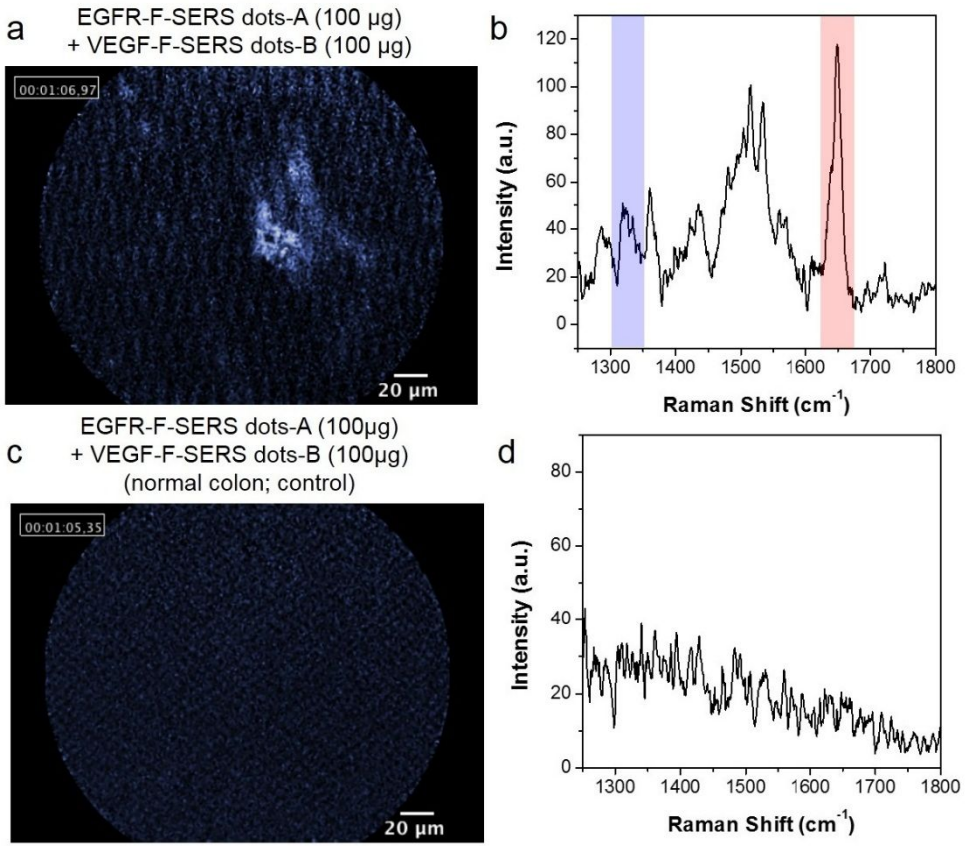

Figure 15. FRES in a real-time endoscopic system.

Mice with CRC (two weeks after 1×10^7 of HT29-effluc cells injection) were investigated for a real-time endoscopic study of the FRES. After spraying 100 μg each of EGFR-F-SERS dots-A and VEGF-F-SERS dots-B, fluorescence signals were found (a), as well as two corresponding Raman signals [RITC (A) and FITC (B)] (b). Whereas, after spraying 100 μg each of EGFR-F-SERS dots-A and VEGF-F-SERS dots-B on normal colons (control), fluorescence (c) or Raman signals (d) were not found.

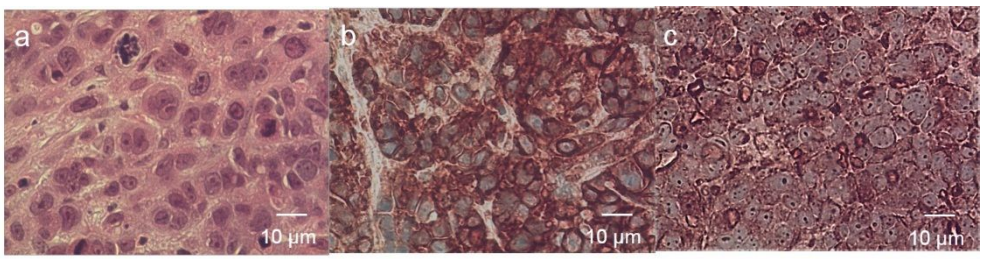

Figure 16. Hematoxylin and eosin (H&E) staining and immunohistochemistry (IHC) results in a real-time endoscopic system.

Tumors exposed to antibody-conjugated F-SERS dots in experiments for Fig. 15 were excised, fixed and sectioned. Tumor cell infiltration was observed on H&E staining (a), and EGFR (b) and VEGF (c) positivity was identified by IHC.

Part IV. Evaluation of sensitivity and lower dose limit of the FRES

Orthotopic CRC xenograft modeling after 5 × 10^6 HT29-effluc cells injection in a tumor-exposed system

The establishment of a xenograft model with small tumors using a lower dose of HT29-effuc cells was attempted. Of 50 studied mice with tumors induced by 5 × 10^6 HT29-effluc cells injection after 1 week, all showed mild-moderate luciferase activity (100%, 50/50). TBR, one week after a 5 × 10^6 HT29-effluc cells injection, showed significantly lower activity compared with the TBR one week after 1 × 10^7 HT29-effluc cells injection (2055 ± 578 vs. 3354 ± 568, $P = 0.044$*; Fig. 17a, b). The largest mean diameter of the colon cancer was 7 mm (range of 5 – 9 mm), and the FRES image for the tumor-exposed system is shown (Fig. 17c).

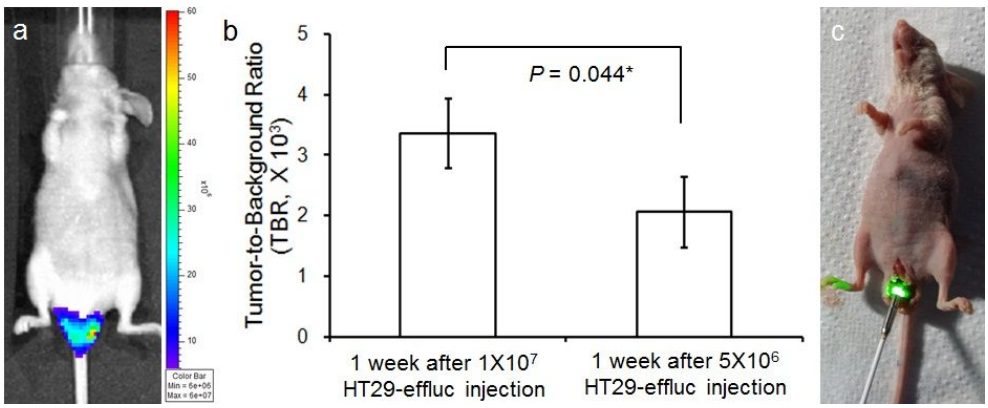

Figure 17. Orthotopic CRC xenograft modeling for small tumors.

After one week of the 5×10^6 HT29-effluc cells injection in mice, bioluminescence imaging (a) showed mild to moderate activity in the colorectal area; A significantly lower TBR was found compared with that for mice one week after the 1×10^7 HT29-effluc cells injection (2,055 ± 578 vs. 3,354 ± 568, $P = 0.044$*) (b). The FRES imaging figure for the tumor-exposed system (c).

Identification of the FRES sensitivity and lower dose limit of antibody-conjugated F-SERS dots in small tumors

Twenty mice with colon cancer were investigated using high doses (EGFR-F-SERS dots-A 100 μg + VEGF-F-SERS dots-B 100 μg), another twenty using medium doses (EGFR-F-SERS dots-A 50 μg + VEGF-F-SERS dots-B 50 μg), and the other ten using low doses (EGFR-F-SERS dots-A 25 μg + VEGF-F-SERS dots-B 25 μg) of antibody-conjugated F-SERS dots for the determination of the sensitivity and the identification of lower dose limit for the FRES. In addition, eight mice were used as controls for normal colon (EGFR-F-SERS dots-A 100 μg + VEGF-F-SERS dots-B 100 μg). The FRES could detect CRC at high and medium doses of antibody-conjugated F-SERS dot in all cases. Definite signals were detected in 80% (16/20) and probable signals in 20% (4/20) of animals for high dose antibody-conjugated F-SERS dot (Fig. 18a, b). And definite signals were detected in 75% (15/20) and probable signals in 25% (5/20) for medium dose antibody-conjugated F-SERS dot (Fig. 18c, d). For low dose antibody-conjugated F-SERS dots group, 50% (5/10) showed definite signals and 30% (3/10) were probable signals. No signal was found for low dose antibody-conjugated F-SERS dot in 20% (2/10) (Fig. 18e, f). Fluorescence and Raman signals were not observed on all control normal colon cases (Fig. 18g, h) (Table 5). CLSM of tumor sections showed definite binding when high, medium and low doses of antibody-conjugated F-SERS dots were used, while binding of antibody-conjugated F-SERS dots on

normal colon was not seen (Fig. 19). Thus, high, medium and low dose antibody-conjugated F-SERS dots specifically bind to tumors in a CRC xenograft model.

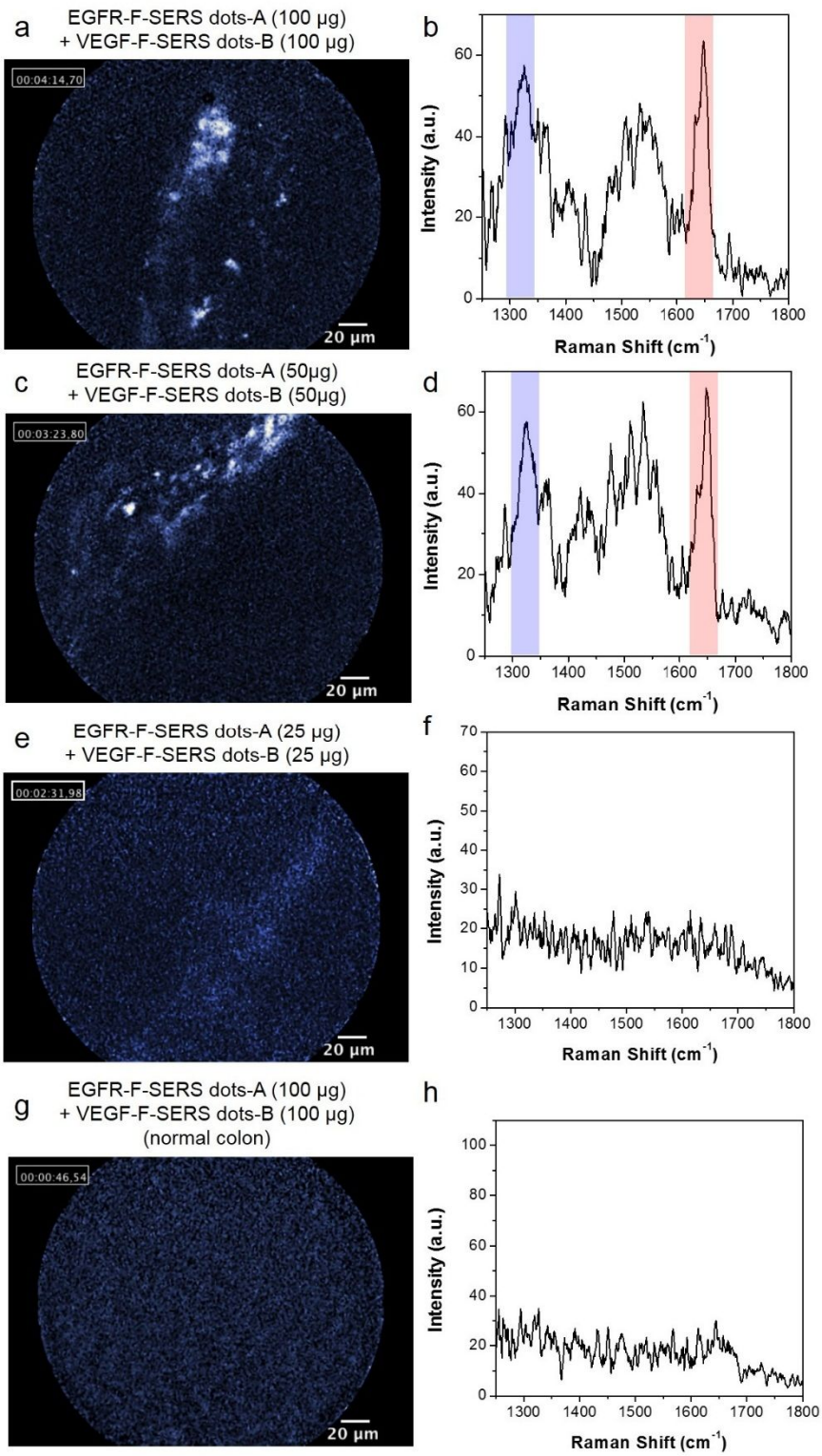
a
EGFR-F-SERS dots-A (100 μg)
+ VEGF-F-SERS dots-B (100 μg)
00:04:14,70
20 μm
b
Intensity (a.u.)
Raman Shift (cm-1)
c
EGFR-F-SERS dots-A (50μg)
+ VEGF-F-SERS dots-B (50μg)
00:03:23,80
20 μm
d
Intensity (a.u.)
Raman Shift (cm-1)
e
EGFR-F-SERS dots-A (25 μg)
+ VEGF-F-SERS dots-B (25 μg)
00:02:31,98
20 μm
f
Intensity (a.u.)
Raman Shift (cm-1)
g
EGFR-F-SERS dots-A (100 μg)
+ VEGF-F-SERS dots-B (100 μg)
(normal colon)
00:00:46,54
20 μm
h
Intensity (a.u.)
Raman Shift (cm-1)

Figure 18. FRES for sensitivity and lower dose limit identification.

After spraying 100 µg (n = 20) or 50 µg (n = 20) of EGFR-F-SERS dots-A and VEGF-F-SERS dots-B onto small tumors in a CRC xenograft model, fluorescence signals were observed (a, c), and two corresponding Raman signals [RITC (A) and FITC (B)] were found (b, d). Whereas, after spraying 25 µg each of EGFR-F-SERS dots-A and VEGF-F-SERS dots-B (n = 10), faint fluorescence signal (e) and no Raman signal (f) was found in some cases (20%, 2/10). On normal colon (control; n = 8), no fluorescence (g) and Raman signal (h) was found corresponding EGFR-F-SERS dots-A and VEGF-F-SERS dots-B.

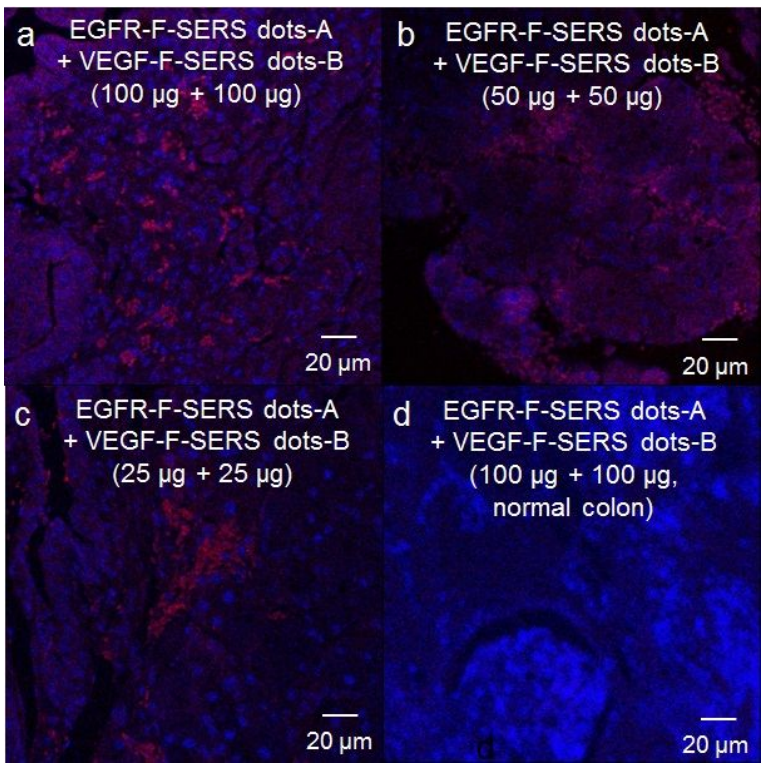

Figure 19. CLSM for sensitivity and lower dose limit identification.

Tumors exposed to antibody-conjugated F-SERS dots in experiments for Fig. 16 were excised, fixed and sectioned. Nuclei were stained with DAPI. CLSM was used for fluorescence signal detection. On 100 µg (a), 50 µg (b) and 25 µg (c) of both antibody-conjugated F-SERS dots sprayed tumors, fluorescence signals were observed. No fluorescence signal was found on 100 µg (d) of antibody-conjugated F-SERS dots sprayed normal colon.

Discussion

We have shown that the FRES is a useful endoscopic tool in an orthotopic CRC xenograft model using antibody-conjugated F-SERS dots. The FRES has advantages in that it allows the fast simultaneous detection of fluorescence and Raman signals. Fluorescence signals were useful for fast tracking of the lesion, and Raman signals were helpful for multiplex targeting (both tumor cell and tumor microenvironment) and quantification. Most of all, we identified that the FRES could be useful for *in vivo* real-time endoscopic system as a practical diagnostic tool. In addition, we confirmed the multiplex targeting ability of the FRES in a subcentimeter-sized colorectal cancer by lowering the spraying dose of antibody-conjugated F-SERS dots according to tumor size and verified sensitivity of the FRES.

The main advantage of the FRES is that it can be easily applied to a conventional endoscopic system, because the FRES was modified an optical fiber bundle probe which can be inserted into an accessory channel of conventional endoscope (*14,25*). When the FRES is applied in routine colonoscopy under clinical conditions, the three combined signals (white source/fluorescence/Raman signals) can be helpful for the multiplex molecular characterization of a suspicious CRC lesion in real-time. Fluorescence-based techniques have many advantages in that they can improve the detection ability of routine colonoscopy, low cost and use a probe that lacks toxicity; however, they also have limitations in that only one

signal can be detected due to its broad bandwidth; also, autofluorescence from tissue leads to false-positive results (*26-28*). In contrast, surface-enhanced Raman spectroscopy (SERS)-based techniques have many advantages such as high sensitivity and multiplex targeting abilities, but show limitations such as a small field of view and limited studied data (*28-31*). In contrast, the FRES can take the advantages of both a large field of view (fluorescence signal) and a multiplex ability (SERS signal) via combined dual-modality, resulting in the rapid and accurate characterization of lesions.

The molecular characterization of CRC is very important for the selection of the most appropriate treatment option and also for patients' prognosis and quality of life if their cancer is at an advanced stage. For CRC, EGFR (anti-EGFR monoclonal antibody: cetuximab) and VEGF (anti-VEGF monoclonal antibody: bevacizumab) targeted therapy is the standard therapy that prolongs the survival in patients with metastatic disease (*32*), and previous studies showed that molecular imaging of EGFR (*33*) and VEGF (*34,35*) can be performed *in vivo.* So we decided our FRES imaging targets as EGFR and VEGF. As EGFR is on cell membrane (tumor cell targeting) (*36*), and VEGF is mainly in extracellular matrix (tumor microenvironment targeting) (*37*), our study results showed simultaneous tumor cell and tumor microenvironment imaging. In addition, our previous pilot study targeting human epidermal growth factor-2 (HER2) and EGFR using HT29-effluc cells xenograft model showed multiplex cellular targeting ability (Fig. 20).

IHC is routinely used for molecular diagnosis. However, IHC can yield false results due to technical and interpretative pitfalls (*38*). Fixation and tissue

processing artifacts, as well as antigen retrieval errors during IHC procedure can hamper the exact evaluation of a tumor's characteristics (*4*). Additionally, 2 – 3 days' delayed evaluation after colonoscopy may cause a loss of optimal treatment time (*39,40*). With the FRES, we can achieve multiple molecular characteristics while performing real-time colonoscopy with high accuracy, resulting in a rapid and effective diagnosis.

For the clinical application of the FRES, stability of the F-SERS dots, signal sensitivity, specificity and the toxicity of nanoparticles are major issues (*41*). Above all, F-SERS dots showed good stability. Fluorescence and Raman signals did not decline or change according to surface modification and antibody conjugation, and emitted fluorescence and Raman signals for more than 1 year after synthesis. In regard to the issue of sensitivity, we performed the FRES study on small tumors (less than 1 cm) and showed that the FRES revealed a similar multiplex targeting ability as that for large tumors (greater than 1 cm). For specificity issue, we performed blocking study and demonstrated that FRES signals were selectively blocked by cold antibodies (Fig. 20). In regard to the toxicity issue, we reduced systemic toxicity by using topical administration method via direct spray of antibody-conjugated F-SERS dots on tumor, bypassing the major disadvantages of intravenous injection: systemic toxicity caused by accumulation in major organs (lung, liver and spleen) (*42-45*); and a decreased tumor targeting ability due to the large size of antibody-conjugated F-SERS dots could be evaded (*46*). In addition, we synthesized a silica shell (nontoxic coating) for the F-SERS dots, which is well known to reduce the toxicity of nanoparticles (*47-49*).

Furthermore, we observed that antibody-conjugated F-SERS dots did not accumulate in the normal colon after washing, further reducing any toxicity towards normal organs. Lastly, the half dose of antibody-conjugated F-SERS dots used for small tumors showed similar FRES results as for a high dose; spraying 50 + 50 μg of antibody-conjugated F-SERS dots (5 nmole) onto a small tumor was found to be acceptable.

One importance of our study is quantification of Raman intensity. As the Raman signal showed high signal intensity, the intensity could be quantified by measuring highest height of Raman signal. *In vitro* study demonstrated that Raman intensity increases according to EGFR-F-SERS dots-A doses, or seeded cell density. In addition, as the standard deviation (SD) of noise from normal colon was equal or less than 10 arbitrary unit (a.u.), we set more than 2× SD (> 20 a.u.; more than 95 percentile) as a probable signal, and more than 3× SD (> 30 a.u.; more than 99.7 percentile) as a definite signal. Moreover, The possibility to detect molecular heterogeneity of the tumor, which is a major obstacle for personalized medicine (*50*), could be evaluated by FRES using quantification of Raman intensity *ex vivo* (Fig. 21).

Our study yielded several limitations. Firstly, because our research was limited to dual targeting, multiplex targeting ability of more than three needs to be investigated in the future study. In addition, as the FRES study showed a large variation in results in spite of the same conditions being used in each experiment

(e.g. Raman intensity range of EGFR-F-SERS dots-A = 350 – 1,250 a.u.; VEGF-F-SERS dots-B = 40 – 220 a.u.) the optimal conditions under which we can get multiplex targeting of the FRES needs to be further evaluated. Lastly, although we showed that a topical spraying dose of F-SERS dots could be reduced for a small tumor, the upper dose limit for antibody-conjugated F-SERS dots in a human body needs to be investigated for any future clinical applications.

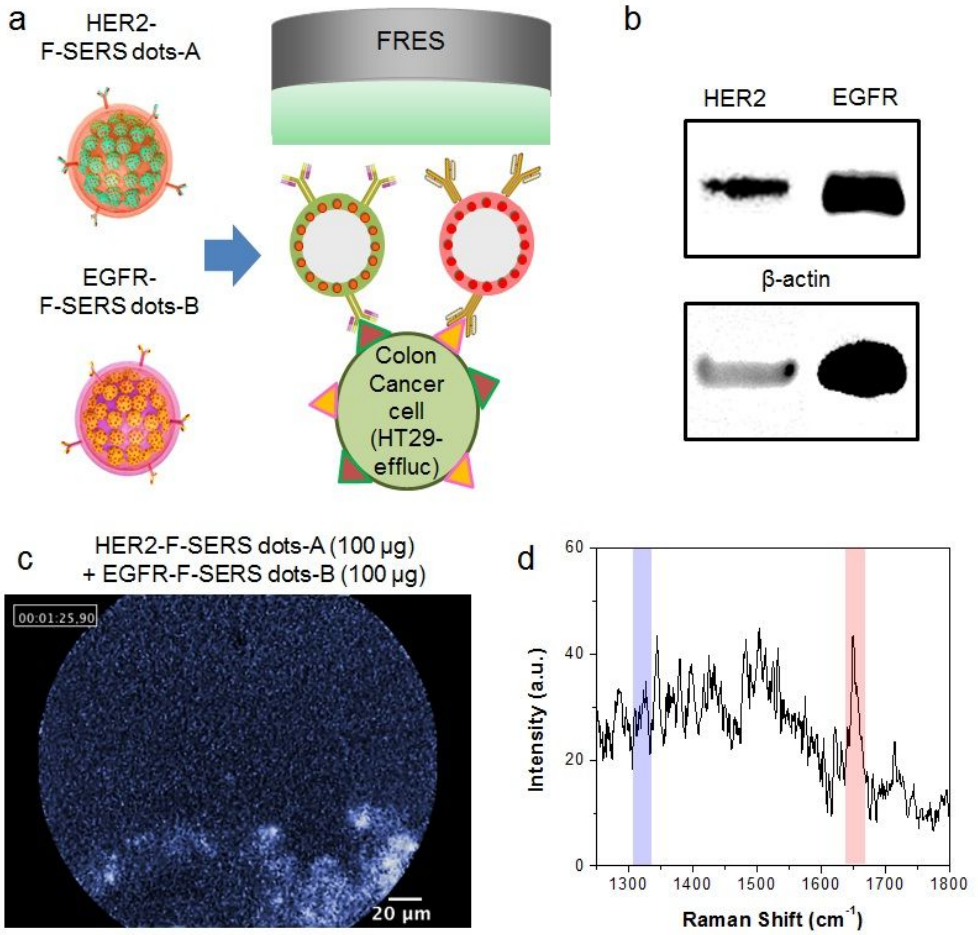

Figure 20. Multiplex cellular targeting of tumor using the FRES.

(a) Schematic illustration of the study. (b) Western blot analysis showed positive human epidermal growth factor receptor-2 (HER2) and EGFR of HT29-effluc cells. FRES result demonstrated that mice with colon cancers (two week after 1×10^7 of HT29-effluc cells injection) demonstrated fluorescence signals (c) and two corresponding Raman signals (d) after spraying 100 μg each of HER2-F-SERS dots-A and EGFR-F-SERS dots-B.

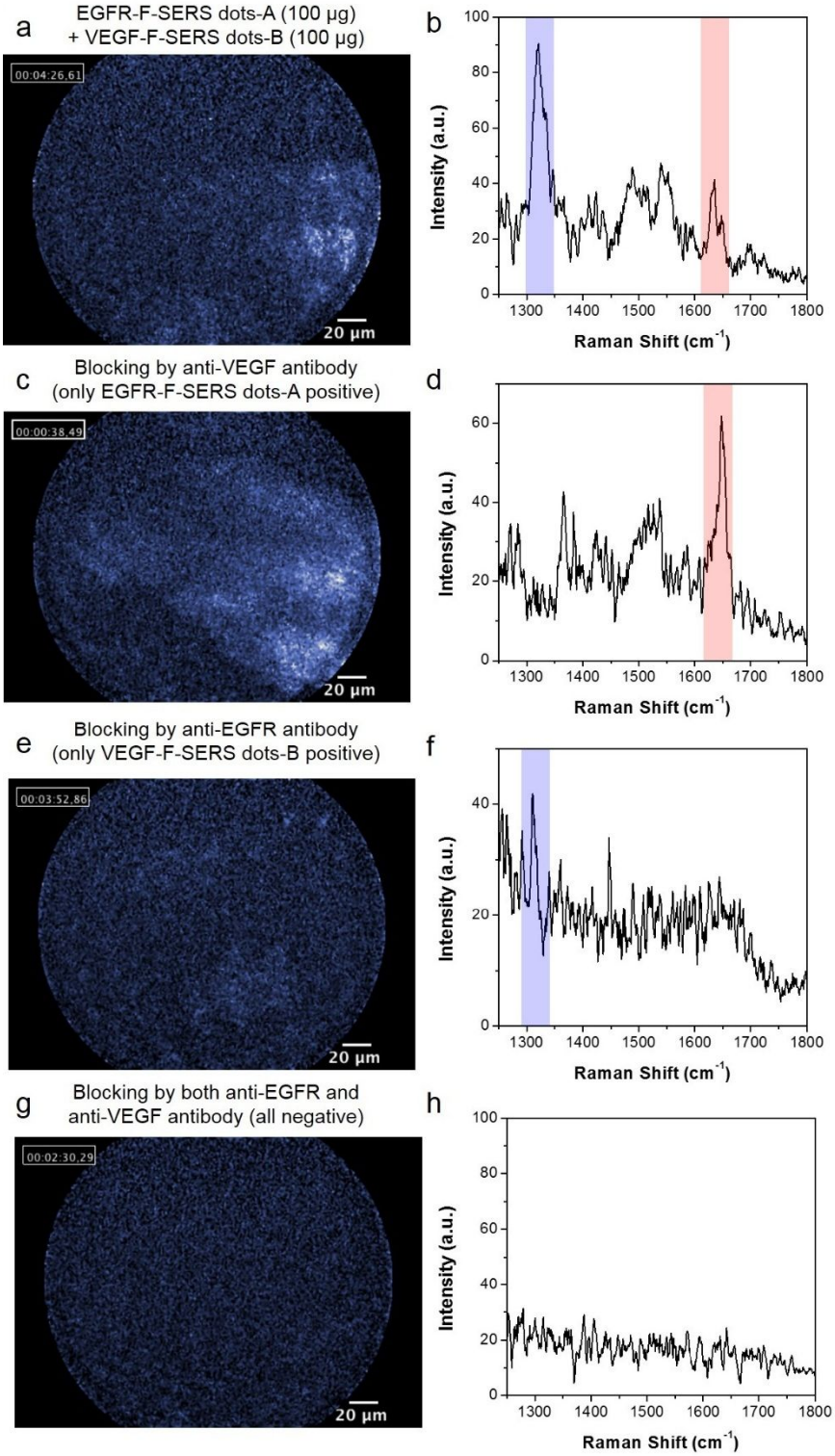
a
EGFR-F-SERS dots-A (100 μg)
+ VEGF-F-SERS dots-B (100 μg)
00:04:26.61
20 μm
b
Intensity (a.u.)
Raman Shift (cm-1)
c
Blocking by anti-VEGF antibody
(only EGFR-F-SERS dots-A positive)
00:00:38.49
20 μm
d
Intensity (a.u.)
Raman Shift (cm-1)
e
Blocking by anti-EGFR antibody
(only VEGF-F-SERS dots-B positive)
00:03:52.86
20 μm
f
Intensity (a.u.)
Raman Shift (cm-1)
g
Blocking by both anti-EGFR and
anti-VEGF antibody (all negative)
00:02:30.29
20 μm
h
Intensity (a.u.)
Raman Shift (cm-1)

Figure 21. Blocking study of the FRES using cold antibodies.

After 2 weeks of 1×10^7 HT29-effluc cells injection orthotopically, tumors were exposed and blocking study was done using cold antibodies (anti-EGFR and/or anti-VEGF antibody) for 10 min. After blocking, 100 μg of antibody-conjugated F-SERS dots (EGFR-F-SERS dots-A and VEGF-F-SERS dots-B) were sprayed. Tumors were investigated by a FRES probe after 10 min of incubation and PBS washing. Tumor without blocking (a, b) showed definite fluorescence signal and two Raman intensities [RITC (A) and FITC (B)]. Single blocking using anti-VEGF antibody (c, d) and anti-EGFR antibody (e, f) demonstrated fluorescence signals, however Raman intensities for FITC (B) and RITC (A) were not found, respectively. Dual blocking by anti-EGFR and anti-VEGF antibodies (g, h) revealed no definite fluorescence and Raman signals.

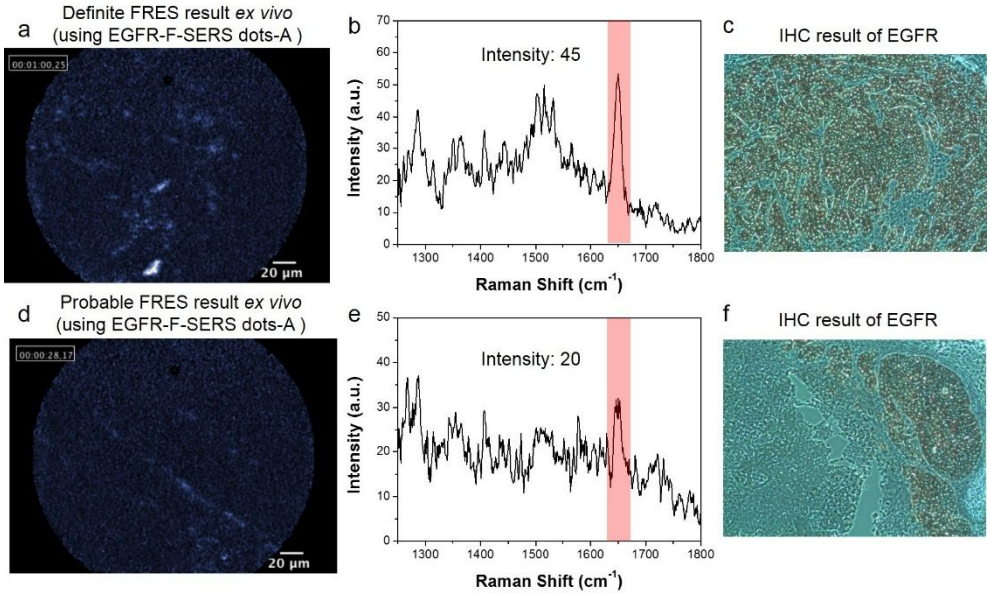

Figure 22. Detection of heterogenous EGFR expression by the FRES *ex vivo*. After 1 week of 1×10^7 HT29-effluc cells subcutaneous injection, tumors were excised, and divided in half. One-hundred μg of EGFR-F-SERS dots-A were sprayed, and investigated by the FRES. Tumors expressing definite fluorescence and Raman intensity (a, b) showed intense EGFR expressions by IHC (c). On the contrary, tumors showing probable fluorescence and Raman intensity (d, e) demonstrated moderate EGFR expressions by IHC (f).

Conclusion

In conclusion, we demonstrated that the FRES can be utilized for multiplex molecular diagnosis, which can be easily applied to current routine endoscopy system. With the FRES, we expect that multiple molecular characteristics of a tumor (tumor cell and tumor microenvironment) can be acquired simultaneously while performing a colonoscopy, and can be effective for the early and most appropriate selection of a treatment option. In addition, the FRES can be applied to small tumors by lowering the dose of topically sprayed F-SERS dots, which can minimize toxicity problem when clinically applied. Besides, Raman signal intensity is quantifiable, which has the possibility to measure the molecular heterogeneity of the tumor. We expect that the FRES will eventually become an appropriate endoscopic technique for the rapid and specific diagnosis of CRC.

Table 1. Summary of nanoparticle tracking analysis (NTA) results for F-SERS dots and antibody-conjugated F-SERS dots

agents	mean size (nm)	standard deviation (SD, nm)
F-SERS dots-A	284.4	60.0
EGFR-F-SERS dots-A	291.0	87.4
F-SERS dots-B	278.1	57.7
VEGF-F-SERS dots-B	296.6	36.9

F-SERS = fluorescence and surface-enhanced Raman scattering; EGFR = epidermal growth factor receptor; VEGF = vascular endothelial growth factor

Table 2. Clinical results of colorectal cancer orthotopic xenograft modeling

time after 1×10^7 HT29-effluc cells injection	survival	anal erosion
1 week	100% (20/20)	35% (7/20)
2 week	70% (14/20)	86% (12/14)

Table 3. Mutiplex targeting ability validation of the FRES

spraying materials	definite signal	probable signal	no signal
EGFR-F-SERS dots-A + VEGF-F-SERS dots-B (100 μg + 100 μg, multiplex targeting)	80% (4/5)	20% (1/5)	0% (0/5)
EGFR-F-SERS dots-A (100 μg, single targeting)	100% (3/3)	0% (0/3)	0% (0/3)
VEGF-F-SERS dots-B (100 μg, single targeting)	100% (3/3)	0% (0/3)	0% (0/3)
BSA-F-SERS dots-A/B (100 μg + 100 μg, control)	0% (0/3)	0% (0/3)	100% (3/3)

FRES = fluorescence-Raman endoscopic system

Table 4. Confirmation of the usefulness of the FRES in a real-time endoscopic system

spraying dose (EGFR-F-SERS dots-A + VEGF-F-SERS dots-B)	definite signal	probable signal	no signal
100 μg + 100 μg	75% (15/20)	25% (5/20)	0% (0/20)
100 μg + 100 μg (normal colon; control)	0% (0/9)	0% (0/9)	100% (9/9)

Table 5. Sensitivity and lower limit dose identification of the FRES

spraying dose (EGFR-F-SERS dots-A + VEGF-F-SERS dots-B)	definite signal	probable signal	no signal
100 μg + 100 μg	80% (16/20)	20% (4/20)	0% (0/20)
50 μg + 50 μg	75% (15/20)	25% (5/20)	0% (0/20)
25 μg + 25 μg	50% (5/10)	30% (3/10)	20% (2/10)
100 μg + 100 μg (normal colon; control)	0% (0/8)	0% (0/8)	100% (8/8)

References

1. Fisher DA, Shergill AK, Early DS, Acosta RD, Chandrasekhara V, Chathadi KV, et al. Role of endoscopy in the staging and management of colorectal cancer. Gastrointest Endosc. 2013;78:8-12.

2. Davila RE, Rajan E, Adler D, Hirota WK, Jacobson BC, Leighton JA, et al. ASGE guideline: the role of endoscopy in the diagnosis, staging, and management of colorectal cancer. Gastrointest Endosc. 2005;61:1-7.

3. Stallmach A, Schmidt C, Watson A, Kiesslich R. An unmet medical need: advances in endoscopic imaging of colorectal neoplasia. J Biophotonics. 2011;4:482-9.

4. Kiesslich R, Goetz M, Hoffman A, Galle PR. New imaging techniques and opportunities in endoscopy. Nat Rev Gastroenterol Hepatol. 2011;8:547-53.

5. Pan Y, Volkmer JP, Mach KE, Rouse RV, Liu JJ, Sahoo D, et al. Endoscopic molecular imaging of human bladder cancer using a CD47 antibody. Sci Transl Med. 2014;6:260ra148.

6. Waldner MJ, Wirtz S, Neufert C, Becker C, Neurath MF. Confocal laser endomicroscopy and narrow-band imaging-aided endoscopy

for in vivo imaging of colitis and colon cancer in mice. Nat Protoc. 2011;6:1471-81.

7. Matousek P, Stone N. Emerging concepts in deep Raman spectroscopy of biological tissue. Analyst. 2009;134:1058-66.

8. Bergholt MS, Zheng W, Ho KY, Yeoh KG, Huang Z. Raman Endoscopy for Objective Diagnosis of Early Cancer in the Gastrointestinal System. J Gastroint Dig Syst. 2013;S1:008

9. Rodriguez-Lorenzo L, Fabris L, Alvarez-Puebla RA. Multiplex optical sensing with surface-enhanced Raman scattering: a critical review. Anal Chim Acta. 2012;745:10-23.

10. Maiti KK, Dinish U, Samanta A, Vendrell M, Soh KS, Park SJ, et al. Multiplex targeted in vivo cancer detection using sensitive near-infrared SERS nanotags. Nano Today. 2012;7:85-93.

11. Nijssen A, Koljenović S, Bakker Schut TC, Caspers PJ, Puppels GJ. Towards oncological application of Raman spectroscopy. J Biophotonics. 2009;2:29-36.

12. Beyer T, Townsend DW, Brun T, Kinahan PE, Charron M, Roddy R, et al. A combined PET/CT scanner for clinical oncology. J Nucl Med. 2000;41:1369-79.

13. Sauter AW, Wehrl HF, Kolb A, Judenhofer MS, Pichler BJ. Combined PET/MRI: one step further in multimodality imaging.

Trends Mol Med. 2010;16:508-15.

14. Dunbar KB, Canto MI. Confocal endomicroscopy. Techniques in Gastrointestinal Endoscopy. 2010;12:90-9.

15. Zavaleta CL, Garai E, Liu JT, Sensarn S, Mandella MJ, Van de Sompel D, et al. A Raman-based endoscopic strategy for multiplexed molecular imaging. Proc Natl Acad Sci USA. 2013;110:E2288-97.

16. Lorusso G, Rüegg C. The tumor microenvironment and its contribution to tumor evolution toward metastasis. Histochem Cell biol. 2008;130:1091-1103.

17. Joyce JA. Therapeutic targeting of the tumor microenvironment. Cancer Cell. 2005;7:513-20.

18. Jeong S, Kim YI, Kang H, Kim G, Cha MG, Chang H, et al. Fluorescence-Raman dual modal endoscopic system for multiplexed molecular diagnostics. Sci Rep. 2015;5:9455.

19. Stöber W, Fink A, Bohn E. Controlled growth of monodisperse silica spheres in the micron size range. Journal of colloid and interface science. 1968;26:62-9.

20. Shimizu M, Deguchi A, Lim JT, Moriwaki H, Kopelovich L, Weinstein IB. (−)-Epigallocatechin gallate and polyphenon E inhibit growth and activation of the epidermal growth factor receptor and human epidermal growth factor receptor-2 signaling pathways in

human colon cancer cells. Clin Cancer Res. 2005;11:2735-46.

21. Lee ES, Im HJ, Kim HS, Youn H, Lee HJ, Kim SU, et al. In vivo brain delivery of v-myc overproduced human neural stem cells via the intranasal pathway: tumor characteristics in the lung of a nude mouse. Mol Imaging. 2014;13:1-10.

22. Rabinovich BA, Ye Y, Etto T, Chen JQ, Levitsky HI, Overwijk WW, et al. Visualizing fewer than 10 mouse T cells with an enhanced firefly luciferase in immunocompetent mouse models of cancer. Proc Natl Acad Sci USA. 2008;105:14342-6.

23. Donigan M, Norcross LS, Aversa J, Colon J, Smith J, Madero-Visbal R, et al. Novel murine model for colon cancer: non-operative trans-anal rectal injection. J Surg Res. 2009;154:299-303.

24. Takahashi T, Morotomi M, Nomoto K. A novel mouse model of rectal cancer established by orthotopic implantation of colon cancer cells. Cancer Sci. 2004;95:514-9.

25. De Palma GD, Staibano S, Siciliano S, Persico M, Masone S, Maione F, et al. In vivo characterisation of superficial colorectal neoplastic lesions with high-resolution probe-based confocal laser endomicroscopy in combination with video-mosaicing: a feasibility study to enhance routine endoscopy. Dig Liver Dis. 2010;42:791-7.

26. Miller SJ, Joshi BP, Feng Y, Gaustad A, Fearon ER, Wang TD. In

vivo fluorescence-based endoscopic detection of colon dysplasia in the mouse using a novel peptide probe. PLoS One. 2011;6:e17384.

27. Mitsunaga M, Kosaka N, Choyke PL, Young MR, Dextras CR, Saud SM, et al. Fluorescence endoscopic detection of murine colitis-associated colon cancer by topically applied enzymatically rapid-activatable probe. Gut. 2013;62:1179-86.

28. Vendrell M, Maiti KK, Dhaliwal K, Chang YT. Surface-enhanced Raman scattering in cancer detection and imaging. Trends Biotechnol. 2013;31:249-57.

29. Kallaway C, Almond LM, Barr H, Wood J, Hutchings J, Kendall C, et al. Advances in the clinical application of Raman spectroscopy for cancer diagnostics. Photodiagnosis Photodyn Ther. 2013;10:207-19.

30. Wallace MB, Kiesslich R. Advances in endoscopic imaging of colorectal neoplasia. Gastroenterology. 2010;138:2140-50.

31. Taketani A, Hariyani R, Ishigaki M, Andriana BB, Sato H. Raman endoscopy for the in situ investigation of advancing colorectal tumors in live model mice. Analyst. 2013;138:4183-90.

32. El Zouhairi M, Charabaty A, Pishvaian MJ. Molecularly targeted therapy for metastatic colon cancer: proven treatments and promising new agents. Gastrointest Cancer Res. 2011;4:15-21.

33. Goetz M, Ziebart A, Foersch S, Vieth M, Waldner MJ, Delaney P, et

al. In vivo molecular imaging of colorectal cancer with confocal endomicroscopy by targeting epidermal growth factor receptor. Gastroenterology. 2010;138:435-46.

34. Foersch S, Kiesslich R, Waldner MJ, Delaney P, Galle PR, Neurath MF, et al. Molecular imaging of VEGF in gastrointestinal cancer in vivo using confocal laser endomicroscopy. Gut. 2010;59:1046-55.

35. Terwisscha van Scheltinga AG, van Dam GM, Nagengast WB, Ntziachristos V, Hollema H, Herek JL, et al. Intraoperative near-infrared fluorescence tumor imaging with vascular endothelial growth factor and human epidermal growth factor receptor 2 targeting antibodies. J Nucl Med. 2011;52:1778-85.

36. Yarden Y. The EGFR family and its ligands in human cancer: signalling mechanisms and therapeutic opportunities. Eur J Cancer. 2001;37:3-8.

37. Park JE, Keller GA, Ferrara N. The vascular endothelial growth factor (VEGF) isoforms: differential deposition into the subepithelial extracellular matrix and bioactivity of extracellular matrix-bound VEGF. Mol Biol Cell. 1993;4:1317-26.

38. Leong AS. Pitfalls in diagnostic immunohistology. Adv Anat Pathol. 2004;11:86-93.

39. Bussolati G, Leonardo E. Technical pitfalls potentially affecting

diagnoses in immunohistochemistry. J Clin Pathol. 2008;61:1184-92.

40. Kast RE, Tucker SC, Killian K, Trexler M, Honn KV, Auner GW. Emerging technology: applications of Raman spectroscopy for prostate cancer. Cancer Metastasis Rev. 2014;33:1-21.

41. Goetz M, Wang TD. Molecular imaging in gastrointestinal endoscopy. Gastroenterology. 2010;138:828-33.

42. Zavaleta CL, Hartman KB, Miao Z, James ML, Kempen P, Thakor AS, et al. Preclinical evaluation of Raman nanoparticle biodistribution for their potential use in clinical endoscopy imaging. Small. 2011;7:2232-40.

43. Thakor AS, Luong R, Paulmurugan R, Lin FI, Kempen P, Zavaleta C, et al. The fate and toxicity of Raman-active silica-gold nanoparticles in mice. Sci Transl Med. 2011;3:79ra33.

44. Liu J, Zuo X, Li C, Yu T, Gu X, Zhou C, et al. In vivo molecular imaging of epidermal growth factor receptor in patients with colorectal neoplasia using confocal laser endomicroscopy. Cancer Lett. 2013;330:200-7.

45. Park Y, Ryu YM, Jung Y, Wang T, Baek Y, Yoon Y, et al. Spraying quantum dot conjugates in the colon of live animals enabled rapid and multiplex cancer diagnosis using endoscopy. ACS Nano. 2014;8:8896-910.

46. Mahmood U. Optical molecular imaging approaches in colorectal cancer. Gastroenterology. 2010;138:419-22.

47. Huh YS, Chung AJ, Erickson D. Surface enhanced Raman spectroscopy and its application to molecular and cellular analysis. Microfluid Nanofluid. 2009;6:285-97.

48. Yang X, Gondikas AP, Marinakos SM, Auffan M, Liu J, Hsu-Kim H, et al. Mechanism of silver nanoparticle toxicity is dependent on dissolved silver and surface coating in Caenorhabditis elegans. Environ Sci Technol. 2011;46:1119-27.

49. Yu KN, Lee SM, Han JY, Park H, Woo MA, Noh MS, et al. Multiplex targeting, tracking, and imaging of apoptosis by fluorescent surface enhanced Raman spectroscopic dots. Bioconjugate chemistry. 2007;18:1155-62.

50. Almendro V, Marusyk A, Polyak K. Cellular heterogeneity and molecular evolution in cancer. Annu Rev Pathol. 2013;8:277-302.

국 문 초 록

대장직장암 마우스 모델에서 형광-라만 동시 내시경 영상을 이용한 실시간 다중복합 생체분자진단

김용일

서울대학교

융합과학기술대학원 분자의학 및 바이오제약학과

목적:

형광 영상을 이용한 내시경 영상은 분자 표적에 대한 빠른 정보를 제공하며, 라만 영상을 이용한 내시경 영상은 다중 분자 표적에 대한 확인을 할 수 있다. 본 연구진은 형광-라만 동시 내시경 장비를 개발하여, 이를 대장직장암 마우스 모델에 적용하고 그 효용성을 확인해 보고자 하였다. 이번 연구에서 우리는 형광-라만 동시 내시경 장비의 다중복합 생체분자표적 감지 (종양 세포와 종양 미세환경 표적), 내시경

모델에의 적용, 장비의 민감도와 라만 영상 강도의 정량화 가능성을 확인해 보았다.

방법:

형광-라만 동시 내시경 장비는 상용화된 공초점 내시경을 개조하여, 형광과 라만 영상을 실시간으로 동시에 확인할 수 있도록 하였다. 또한 표피생장인자 수용체(epidermal growth factor receptor, EGFR)와 혈관내피성장인자(vascular endothelial growth factor, VEGF)를 발현하는 대장직장암 마우스 모델을 만들었다. 대장직장암 마우스 모델에 항체(EGFR 과 VEGF)를 도입한 형광과 표면 증강 라만을 함께 내는 나노입자(fluorescence and surface-enhanced Raman scattering nanoprobes, F-SERS dots)를 분무하여 다중복합 생체분자진단이 가능한지 확인하여 보았다. 또한 형광-라만 동시 내시경 장비를 이용한 마우스 내시경 모델을 확립하여 이에 대한 다중복합 생체분자진단 가능성을 확인하였다. 더욱이 1 센티미터 이하의 작은 대장직장암 마우스 모델을 만들어 형광과 표면 증강 라만을 함께 내는 나노입자의 용량을 줄였을 경우 형광-라만 동시 내시경 장비의 민감도를 확인해 보았다.

결과:

형광과 라만 동시 내시경 영상을 대장직장암 마우스 모델에서 확인할 수 있었다. 대장암의 복합 분자 신호(EGFR 과 VEGF)는 형광-라만 동시 내시경 영상에서 형광 영상[Alexa Flour (AF) 610]을 이용해 빠른 신호 확인이 가능하였으며, 라만 영상[rhodamine B isothiocyanate (RITC) 와 fluorescein isothiocyanate (FITC)]을 이용해 다중 분자 신호를 감지할 수 있었다. 또한 형광-라만 동시 내시경 영상은 종양을 노출시킨 경우 뿐만 아니라, 실시간 내시경 검사에서도 다중복합 생체분자 진단이 가능하였다. 형광-라만 동시 내시경 영상의 유용성은 1 센티미터 이하의 종양에서도 확인할 수 있었으며, 나노입자의 용량을 반으로 줄여도 민감도에 큰 차이가 없었다. 라만 신호의 강도는 라만 신호의 높이를 측정하여 정량화 할 수 있었고, F-SERS dot의 농도 증가에 따라, 그리고 세포의 밀도와 분자 특성 발현 증가에 따라 증가하는 경향을 보였다.

결론:

우리는 형광-라만 동시 내시경을 이용해 빠른 신호 확인과 다중 분자 신호 감지가 가능함을 생체 내에서 확인하였다. 종양 세포막에 존재하는 EGFR을 통해 종양 세포 영상을 획득하고, 세포 외 기질에 존재하는 VEGF를 통해 종양 미세환경 영상을 획득함으로써 다중복합 생체분자 영상을 실시간으로 얻을 수 있었다. 또한 대장직장암 모델에서 실제

내시경 검사법을 형광-라만 동시 내시경을 이용해 구현하여, 다중 분자 신호 감지가 가능함을 보였다. 더욱이 형광-라만 동시 내시경의 민감도가 종양 크기 1 cm 이하이며, 나노입자 농도 5 나노몰 정도임을 확인하였다. 나노입자의 독성은 나노입자의 무독성 코팅, 국부 분무, 그리고 종양 크기에 따른 나노입자의 용량 감소 등을 통해 감쇄할 수 있어, 우리의 형광-라만 동시 내시경 장비를 인체에 쉽게 적용 할 수 있을 것으로 기대한다. 또한 형광-라만 동시 내시경을 이용할 경우 라만 신호의 강도 계산을 통해 종양의 이질적인 분자 특성을 정량화할 수 있는 가능성을 보였다.

주요어: 형광영상, 라만영상, 다중 표적화, 내시경, 대장암, 표면 증강 라만 산란

학번: 2009-24111